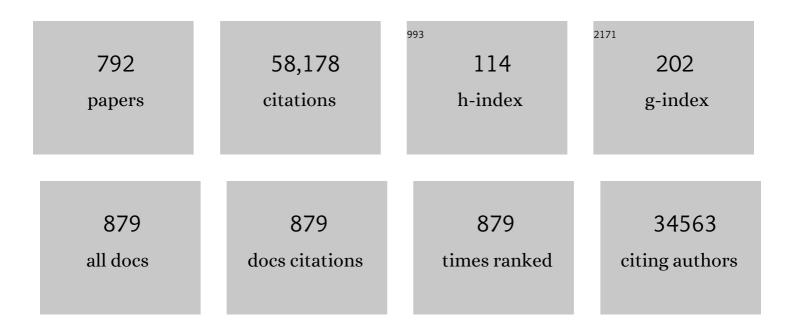
List of Publications by Year in descending order

Source: https://exaly.com/author-pdf/117338/publications.pdf Version: 2024-02-01



#	Article	IF	CITATIONS
1	The Catalytic Valorization of Lignin for the Production of Renewable Chemicals. Chemical Reviews, 2010, 110, 3552-3599.	23.0	3,704
2	Paving the Way for Lignin Valorisation: Recent Advances in Bioengineering, Biorefining and Catalysis. Angewandte Chemie - International Edition, 2016, 55, 8164-8215.	7.2	1,576
3	Catalytic Dehydrogenation of Light Alkanes on Metals and Metal Oxides. Chemical Reviews, 2014, 114, 10613-10653.	23.0	1,473
4	Chemistry, spectroscopy and the role of supported vanadium oxides in heterogeneous catalysis. Catalysis Today, 2003, 78, 25-46.	2.2	825
5	Beyond Mechanical Recycling: Giving New Life to Plastic Waste. Angewandte Chemie - International Edition, 2020, 59, 15402-15423.	7.2	809
6	The renaissance of iron-based Fischer–Tropsch synthesis: on the multifaceted catalyst deactivation behaviour. Chemical Society Reviews, 2008, 37, 2758.	18.7	730
7	Surface Chemistry and Spectroscopy of Chromium in Inorganic Oxides. Chemical Reviews, 1996, 96, 3327-3350.	23.0	729
8	Fluid catalytic cracking: recent developments on the grand old lady of zeolite catalysis. Chemical Society Reviews, 2015, 44, 7342-7370.	18.7	716
9	New insights into the structure and composition of technical lignins: a comparative characterisation study. Green Chemistry, 2016, 18, 2651-2665.	4.6	648
10	Structure and reactivity of surface vanadium oxide species on oxide supports. Applied Catalysis A: General, 1997, 157, 67-90.	2.2	636
11	Catalytic processes monitored at the nanoscale with tip-enhanced Raman spectroscopy. Nature Nanotechnology, 2012, 7, 583-586.	15.6	570
12	Recent trends and fundamental insights in the methanol-to-hydrocarbons process. Nature Catalysis, 2018, 1, 398-411.	16.1	507
13	Formation, Molecular Structure, and Morphology of Humins in Biomass Conversion: Influence of Feedstock and Processing Conditions. ChemSusChem, 2013, 6, 1745-1758.	3.6	482
14	The Production of Propene Oxide:Â Catalytic Processes and Recent Developments. Industrial & Engineering Chemistry Research, 2006, 45, 3447-3459.	1.8	456
15	Stability and Reactivity of ϵâ^'χâ^'Î, Iron Carbide Catalyst Phases in Fischerâ^'Tropsch Synthesis: Controlling μ <sub>C</sub> . Journal of the American Chemical Society, 2010, 132, 14928-14941.	6.6	426
16	Heterogeneities of individual catalyst particles in space and time as monitored by spectroscopy. Nature Chemistry, 2012, 4, 873-886.	6.6	392
17	Unravelling structure sensitivity in CO2 hydrogenation over nickel. Nature Catalysis, 2018, 1, 127-134.	16.1	386
18	Nanoscale chemical imaging of a working catalyst by scanning transmission X-ray microscopy. Nature, 2008, 456, 222-225.	13.7	376

#	Article	IF	CITATIONS
19	Chemocatalytic Conversion of Ethanol into Butadiene and Other Bulk Chemicals. ChemSusChem, 2013, 6, 1595-1614.	3.6	371
20	The renaissance of the Sabatier reaction and its applications on Earth and in space. Nature Catalysis, 2019, 2, 188-197.	16.1	369
21	Alkane dehydrogenation over supported chromium oxide catalysts. Catalysis Today, 1999, 51, 223-232.	2.2	344
22	Product shape selectivity dominates the Methanol-to-Olefins (MTO) reaction over H-SAPO-34 catalysts. Journal of Catalysis, 2009, 264, 77-87.	3.1	344
23	Chemical Imaging of Spatial Heterogeneities in Catalytic Solids at Different Length and Time Scales. Angewandte Chemie - International Edition, 2009, 48, 4910-4943.	7.2	339
24	In Situ Spectroscopic Investigation of Molecular Structures of Highly Dispersed Vanadium Oxide on Silica under Various Conditions. Journal of Physical Chemistry B, 1998, 102, 10842-10852.	1.2	338
25	Bis(μ-oxo)dicopper in Cu-ZSM-5 and Its Role in the Decomposition of NO: A Combined in Situ XAFS, UVâ°'Visâ°'Near-IR, and Kinetic Study. Journal of the American Chemical Society, 2003, 125, 7629-7640.	6.6	338
26	Recent advances in zeolite chemistry and catalysis. Chemical Society Reviews, 2015, 44, 7022-7024.	18.7	333
27	Determining the active site in a catalytic process: Operando spectroscopy is more than a buzzword. Physical Chemistry Chemical Physics, 2003, 5, 4351.	1.3	321
28	Confirmation of Isolated Cu <sup>2+</sup> Ions in SSZ-13 Zeolite as Active Sites in NH <sub>3</sub> -Selective Catalytic Reduction. Journal of Physical Chemistry C, 2012, 116, 4809-4818.	1.5	310
29	Space―and Timeâ€Resolved Inâ€situ Spectroscopy on the Coke Formation in Molecular Sieves: Methanolâ€toâ€Olefin Conversion over Hâ€ZSMâ€5 and Hâ€6APOâ€34. Chemistry - A European Journal, 2008, 1 11320-11327.	l 4j.7	303
30	Local Environment and Nature of Cu Active Sites in Zeolite-Based Catalysts for the Selective Catalytic Reduction of NO <sub><i>x</i></sub> . ACS Catalysis, 2013, 3, 413-427.	5.5	301
31	A New Templated Ordered Structure with Combined Micro- and Mesopores and Internal Silica Nanocapsules. Journal of Physical Chemistry B, 2002, 106, 5873-5877.	1.2	286
32	Ruthenium-catalyzed hydrogenation of levulinic acid: Influence of the support and solvent on catalyst selectivity and stability. Journal of Catalysis, 2013, 301, 175-186.	3.1	281
33	Shale Gas Revolution: An Opportunity for the Production of Biobased Chemicals?. Angewandte Chemie - International Edition, 2013, 52, 11980-11987.	7.2	278
34	High performing and stable supported nano-alloys for the catalytic hydrogenation of levulinic acid to I <sup>3</sup> -valerolactone. Nature Communications, 2015, 6, 6540.	5.8	275
35	Complexity behind CO <sub>2</sub> Capture on NH <sub>2</sub> -MIL-53(Al). Langmuir, 2011, 27, 3970-3976.	1.6	274
36	CoMo sulfide-catalyzed hydrodeoxygenation of lignin model compounds: An extended reaction network for the conversion of monomeric and dimeric substrates. Journal of Catalysis, 2012, 285, 315-323.	3.1	270

#	Article	IF	CITATIONS
37	Snapshots of a working catalyst: possibilities and limitations of in situ spectroscopy in the field of heterogeneous catalysis. Chemical Communications, 2002, , 97-110.	2.2	266
38	Thermally Stable and Regenerable Platinum–Tin Clusters for Propane Dehydrogenation Prepared by Atom Trapping on Ceria. Angewandte Chemie - International Edition, 2017, 56, 8986-8991.	7.2	262
39	A combined in situ time-resolved UV–Vis, Raman and high-energy resolution X-ray absorption spectroscopy study on the deactivation behavior of Pt and PtSn propane dehydrogenation catalysts under industrial reaction conditions. Journal of Catalysis, 2010, 276, 268-279.	3.1	256
40	Morphology-dependent zeolite intergrowth structures leading to distinct internal and outer-surface molecular diffusion barriers. Nature Materials, 2009, 8, 959-965.	13.3	251
41	Conversion of Methane to Benzene over Transition Metal Ion ZSM-5 Zeolites. Journal of Catalysis, 1998, 175, 338-346.	3.1	250
42	Catalytic Lignin Valorization Process for the Production of Aromatic Chemicals and Hydrogen. ChemSusChem, 2012, 5, 1602-1609.	3.6	248
43	Coke Formation during the Methanolâ€ŧoâ€Olefin Conversion: In Situ Microspectroscopy on Individual Hâ€ZSMâ€5 Crystals with Different BrÃ,nsted Acidity. Chemistry - A European Journal, 2011, 17, 2874-2884.	1.7	244
44	Implementation of a combined SAXS/WAXS/QEXAFS set-up for time-resolved <i>in situ</i> experiments. Journal of Synchrotron Radiation, 2008, 15, 632-640.	1.0	243
45	Isolated Cu <sup>2+</sup> ions: active sites for selective catalytic reduction of NO. Chemical Communications, 2011, 47, 800-802.	2.2	243
46	Selective Catalytic Reduction of NO with NH3over Supported Vanadia Catalysts. Journal of Catalysis, 1996, 161, 211-221.	3.1	232
47	Spectroscopy and coordination chemistry of cobalt in molecular sieves. Microporous and Mesoporous Materials, 1998, 22, 165-178.	2.2	229
48	Structure–performance descriptors and the role of Lewis acidity in the methanol-to-propylene process. Nature Chemistry, 2018, 10, 804-812.	6.6	221
49	The concept of active site in heterogeneous catalysis. Nature Reviews Chemistry, 2022, 6, 89-111.	13.8	218
50	Platinumâ€Promoted Ga/Al <sub>2</sub> O <sub>3</sub> as Highly Active, Selective, and Stable Catalyst for the Dehydrogenation of Propane. Angewandte Chemie - International Edition, 2014, 53, 9251-9256.	7.2	215
51	Combining operando techniques in one spectroscopic-reaction cell: New opportunities for elucidating the active site and related reaction mechanism in catalysis. Catalysis Today, 2006, 113, 3-15.	2.2	189
52	Co <sub>3</sub> O <sub>4</sub> –SiO <sub>2</sub> Nanocomposite: A Very Active Catalyst for CO Oxidation with Unusual Catalytic Behavior. Journal of the American Chemical Society, 2011, 133, 11279-11288.	6.6	189
53	Combined DRS–RS–EXAFS–XANES–TPR study of supported chromium catalysts. Journal of the Chemical Society, Faraday Transactions, 1995, 91, 3245-3253.	1.7	188
54	Role of Sn in the Regeneration of Pt/γ-Al <sub>2</sub> O <sub>3</sub> Light Alkane Dehydrogenation Catalysts. ACS Catalysis, 2016, 6, 2257-2264.	5.5	188

#	Article	IF	CITATIONS
55	Olefin polymerization over supported chromium oxide catalysts. Catalysis Today, 1999, 51, 215-221.	2.2	185
56	NaYF <sub>4</sub> :Er <sup>3+</sup> ,Yb <sup>3+</sup> /SiO <sub>2</sub> Core/Shell Upconverting Nanocrystals for Luminescence Thermometry up to 900 K. Journal of Physical Chemistry C, 2017, 121, 3503-3510.	1.5	185
57	Determining the storage, availability and reactivity of NH <sub>3</sub> within Cu-Chabazite-based Ammonia Selective Catalytic Reduction systems. Physical Chemistry Chemical Physics, 2014, 16, 1639-1650.	1.3	181
58	Carbon Nanofiber Supported Transitionâ€Metal Carbide Catalysts for the Hydrodeoxygenation of Guaiacol. ChemCatChem, 2013, 5, 2964-2972.	1.8	180
59	Recent progress in diffuse reflectance spectroscopy of supported metal oxide catalysts. Catalysis Today, 1999, 49, 441-451.	2.2	173
60	Infrared and Raman imaging of heterogeneous catalysts. Chemical Society Reviews, 2010, 39, 4615.	18.7	170
61	Initial Carbon–Carbon Bond Formation during the Early Stages of the Methanolâ€toâ€Olefin Process Proven by Zeoliteâ€Trapped Acetate and Methyl Acetate. Angewandte Chemie - International Edition, 2016, 55, 15840-15845.	7.2	170
62	ZrO <sub>2</sub> Is Preferred over TiO <sub>2</sub> as Support for the Ru-Catalyzed Hydrogenation of Levulinic Acid to Î <sup>3</sup> -Valerolactone. ACS Catalysis, 2016, 6, 5462-5472.	5.5	169
63	A quantitative diffuse reflectance spectroscopy study of supported chromium catalysts. The Journal of Physical Chemistry, 1993, 97, 4756-4763.	2.9	168
64	Title is missing!. Catalysis Letters, 1998, 52, 31-36.	1.4	168
65	Plugged hexagonal templated silica: a unique micro- and mesoporous composite material with internal silica nanocapsulesElectronic supplementary information (ESI) available: Fig. S1: X-ray diffractogram of a PHTS material. Fig. S2: TEM images of SBA-15 and PHTS-2. Fig. S3: hydrothermal stabilities. See http://www.rsc.org/suppdata/cc/b2/b201424f/. Chemical Communications. 2002 1010-1011.	2.2	168
66	MCM-48-Supported Vanadium Oxide Catalysts, Prepared by the Molecular Designed Dispersion of VO(acac)2: A Detailed Study of the Highly Reactive MCM-48 Surface and the Structure and Activity of the Deposited VOx. Journal of Catalysis, 2001, 197, 160-171.	3.1	166
67	In Situ X-ray Absorption of Co/Mn/TiO2Catalysts for Fischerâ^'Tropsch Synthesis. Journal of Physical Chemistry B, 2004, 108, 16201-16207.	1.2	165
68	Glycerol Etherification over Highly Active CaOâ€Based Materials: New Mechanistic Aspects and Related Colloidal Particle Formation. Chemistry - A European Journal, 2008, 14, 2016-2024.	1.7	161
69	Local and long range order in promoted iron-based Fischer–Tropsch catalysts: A combined in situ X-ray absorption spectroscopy/wide angle X-ray scattering study. Journal of Catalysis, 2009, 262, 244-256.	3.1	160
70	Liquid-phase reforming and hydrodeoxygenation as a two-step route to aromatics from lignin. Green Chemistry, 2013, 15, 3049.	4.6	159
71	Wege zur Verwertung von Lignin: Fortschritte in der Biotechnik, der Bioraffination und der Katalyse. Angewandte Chemie, 2016, 128, 8296-8354.	1.6	159
72	EXAFS as a tool to interrogate the size and shape of mono and bimetallic catalyst nanoparticles. Physical Chemistry Chemical Physics, 2010, 12, 5562.	1.3	157

#	Article	IF	CITATIONS
73	Aerobic oxidation of cyclohexane by gold-based catalysts: New mechanistic insight by thorough product analysis. Journal of Catalysis, 2010, 270, 16-25.	3.1	156
74	Transition metal catalyzed oxidation of Alcell lignin, soda lignin, and lignin model compounds in ionic liquids. Green Chemistry, 2010, 12, 1225.	4.6	153
75	Spatial and temporal exploration of heterogeneous catalysts with synchrotron radiation. Nature Reviews Materials, 2018, 3, 324-340.	23.3	153
76	Cu-ZSM-5 Zeolites for the Formation of Methanol from Methane and Oxygen: Probing the Active Sites and Spectator Species. Catalysis Letters, 2010, 138, 14-22.	1.4	152
77	Envisaging the Physicochemical Processes during the Preparation of Supported Catalysts:Â Raman Microscopy on the Impregnation of Mo onto Al2O3Extrudates. Journal of the American Chemical Society, 2004, 126, 14548-14556.	6.6	150
78	Mesopore formation in zeolite H-SSZ-13 by desilication with NaOH. Microporous and Mesoporous Materials, 2010, 132, 384-394.	2.2	150
79	Surface- and Tip-Enhanced Raman Spectroscopy in Catalysis. Journal of Physical Chemistry Letters, 2016, 7, 1570-1584.	2.1	149
80	Propene epoxidation over Au/Ti-SBA-15 catalysts. Journal of Catalysis, 2007, 248, 235-248.	3.1	147
81	Phosphorus promotion and poisoning in zeolite-based materials: synthesis, characterisation and catalysis. Chemical Society Reviews, 2015, 44, 7406-7428.	18.7	147
82	Identification of a diagnostic structural motif reveals a new reaction intermediate and condensation pathway in kraft lignin formation. Chemical Science, 2018, 9, 6348-6360.	3.7	143
83	Conversion of Methane to Benzene over Transition Metal Ion ZSM-5 Zeolites. Journal of Catalysis, 1998, 175, 347-351.	3.1	142
84	Chemical imaging of catalytic solids with synchrotron radiation. Chemical Society Reviews, 2010, 39, 4656.	18.7	141
85	Subâ€Second Timeâ€Resolved Surfaceâ€Enhanced Raman Spectroscopy Reveals Dynamic CO Intermediates during Electrochemical CO <sub>2</sub> Reduction on Copper. Angewandte Chemie - International Edition, 2021, 60, 16576-16584.	7.2	141
86	Effect of water vapor on the molecular structures of supported vanadium oxide catalysts at elevated temperatures. Journal of Molecular Catalysis A, 1996, 110, 41-54.	4.8	140
87	Determining the location and nearest neighbours of aluminium in zeolites with atom probe tomography. Nature Communications, 2015, 6, 7589.	5.8	139
88	The Role of Gold in Gold-Titania Epoxidation Catalysts. Angewandte Chemie - International Edition, 2005, 44, 1115-1118.	7.2	138
89	Lignin up for break-down. Nature Chemistry, 2014, 6, 1035-1036.	6.6	138
90	Characterization of Al2O3-Supported Manganese Oxides by Electron Spin Resonance and Diffuse Reflectance Spectroscopy. Journal of Physical Chemistry B, 1997, 101, 309-316.	1.2	135

#	Article	IF	CITATIONS
91	Influence of acid–base properties on the Lebedev ethanol-to-butadiene process catalyzed by SiO <sub>2</sub> –MgO materials. Catalysis Science and Technology, 2015, 5, 2869-2879.	2.1	135
92	Structural characterization of <sup>13</sup> C-enriched humins and alkali-treated <sup>13</sup> C humins by 2D solid-state NMR. Green Chemistry, 2015, 17, 4383-4392.	4.6	134
93	Molybdenum Speciation and its Impact on Catalytic Activity during Methane Dehydroaromatization in Zeolite ZSMâ€5 as Revealed by Operando Xâ€Ray Methods. Angewandte Chemie - International Edition, 2016, 55, 5215-5219.	7.2	133
94	Fundamental Studies of Butane Oxidation over Model-Supported Vanadium Oxide Catalysts: Molecular Structure-Reactivity Relationships. Journal of Catalysis, 1997, 170, 75-88.	3.1	132
95	Catalytic activity in individual cracking catalyst particles imaged throughout different life stages by selective staining. Nature Chemistry, 2011, 3, 862-867.	6.6	132
96	In Situ Raman Spectroscopy of Supported Transition Metal Oxide Catalysts:Â18O2â^'16O2Isotopic Labeling Studies. Journal of Physical Chemistry B, 2000, 104, 7382-7387.	1.2	131
97	Changing active sites in Cu–CHA catalysts: deNOx selectivity as a function of the preparation method. Microporous and Mesoporous Materials, 2013, 166, 144-152.	2.2	131
98	An operando optical fiber UV–vis spectroscopic study of the catalytic decomposition of NO and N2O over Cu-ZSM-5. Journal of Catalysis, 2003, 220, 500-512.	3.1	129
99	Inâ€situ Scanning Transmission Xâ€Ray Microscopy of Catalytic Solids and Related Nanomaterials. ChemPhysChem, 2010, 11, 951-962.	1.0	129
100	Infrared and Raman spectroscopic study of pH-induced structural changes of l-histidine in aqueous environment. Vibrational Spectroscopy, 2005, 39, 114-125.	1.2	128
101	Unraveling the Crystallization Mechanism of CoAPO-5 Molecular Sieves under Hydrothermal Conditions. Journal of the American Chemical Society, 2005, 127, 14454-14465.	6.6	128
102	Surface Acidity and Basicity of La2O3, LaOCl, and LaCl3Characterized by IR Spectroscopy, TPD, and DFT Calculations. Journal of Physical Chemistry B, 2004, 108, 15770-15781.	1.2	127
103	Adding a third dimension to operando spectroscopy: a combined UV-Vis, Raman and XAFS setup to study heterogeneous catalysts under working conditions. Chemical Communications, 2005, , 3015.	2.2	124
104	Life and death of a single catalytic cracking particle. Science Advances, 2015, 1, e1400199.	4.7	124
105	Understanding carbon dioxide activation and carbon–carbon coupling over nickel. Nature Communications, 2019, 10, 5330.	5.8	124
106	Chemical deactivation of Cu-SSZ-13 ammonia selective catalytic reduction (NH3-SCR) systems. Applied Catalysis B: Environmental, 2014, 154-155, 339-349.	10.8	123
107	Hydration effects on the molecular structure of silica-supported vanadium oxide catalysts: A combined IR, Raman, UV–vis and EXAFS study. Vibrational Spectroscopy, 2007, 43, 140-151.	1.2	122
108	Insights into the Activity and Deactivation of the Methanol-to-Olefins Process over Different Small-Pore Zeolites As Studied with Operando UV–vis Spectroscopy. ACS Catalysis, 2017, 7, 4033-4046.	5.5	122

#	Article	IF	CITATIONS
109	Intergrowth Structure of Zeolite Crystals as Determined by Optical and Fluorescence Microscopy of the Templateâ€Removal Process. Angewandte Chemie - International Edition, 2007, 46, 7228-7231.	7.2	120
110	Diffuse reflectance spectroscopy study of the thermal genesis and molecular structure of chromium-supported catalysts. The Journal of Physical Chemistry, 1994, 98, 579-584.	2.9	119
111	The role of tungsten oxide in the selective hydrogenolysis of glycerol to 1,3-propanediol over Pt/WOx/Al2O3. Applied Catalysis B: Environmental, 2017, 204, 260-272.	10.8	119
112	Nonuniform Catalytic Behavior of Zeolite Crystals as Revealed by In Situ Optical Microspectroscopy. Angewandte Chemie - International Edition, 2007, 46, 3652-3655.	7.2	118
113	Separation and Purification of Hydrocarbons with Porous Materials. Angewandte Chemie - International Edition, 2021, 60, 18930-18949.	7.2	118
114	Lignin Solubilization and Aqueous Phase Reforming for the Production of Aromatic Chemicals and Hydrogen. ChemSusChem, 2011, 4, 369-378.	3.6	117
115	Nanosheets of Nonlayered Aluminum Metal–Organic Frameworks through a Surfactantâ€Assisted Method. Advanced Materials, 2018, 30, e1707234.	11.1	117
116	Spatially resolved UV–vis microspectroscopy on the preparation of alumina-supported Co Fischer–Tropsch catalysts: Linking activity to Co distribution and speciation. Journal of Catalysis, 2006, 242, 287-298.	3.1	116
117	Visualizing the Crystal Structure and Locating the Catalytic Activity of Micro―and Mesoporous ZSMâ€5 Zeolite Crystals by Using In Situ Optical and Fluorescence Microscopy. Chemistry - A European Journal, 2008, 14, 1718-1725.	1.7	116
118	Preface: recent advances in the in-situ characterization of heterogeneous catalysts. Chemical Society Reviews, 2010, 39, 4557.	18.7	116
119	Trimodal Porous Hierarchical SSZ-13 Zeolite with Improved Catalytic Performance in the Methanol-to-Olefins Reaction. ACS Catalysis, 2016, 6, 2163-2177.	5.5	116
120	Finned zeolite catalysts. Nature Materials, 2020, 19, 1074-1080.	13.3	116
121	Mechanistic Study into the Direct Epoxidation of Propene over Gold/Titania Catalysts. Journal of Physical Chemistry B, 2005, 109, 19309-19319.	1.2	113
122	Influence of the Reaction Temperature on the Nature of the Active and Deactivating Species during Methanol to Olefins Conversion over H-SSZ-13. ACS Catalysis, 2015, 5, 992-1003.	5.5	112
123	X-ray Absorption Spectroscopy of Mn/Co/TiO2Fischerâ~'Tropsch Catalysts:Â Relationships between Preparation Method, Molecular Structure, and Catalyst Performance. Journal of Physical Chemistry B, 2006, 110, 8626-8639.	1.2	111
124	Insight into the Effect of Water on the Methanol-to-Olefins Conversion in H-SAPO-34 from Molecular Simulations and in Situ Microspectroscopy. ACS Catalysis, 2016, 6, 1991-2002.	5.5	110
125	Effect of Preparation Method and CuO Promotion in the Conversion of Ethanol into 1,3â€Butadiene over SiO <sub>2</sub> –MgO Catalysts. ChemSusChem, 2014, 7, 2505-2515.	3.6	109
126	Characterization and Comparison of Fast Pyrolysis Bio-oils from Pinewood, Rapeseed Cake, and Wheat Straw Using <sup>13</sup> C NMR and Comprehensive GC × GC. ACS Sustainable Chemistry and Engineering, 2016, 4, 4974-4985.	3.2	109

#	Article	IF	CITATIONS
127	Structure Sensitivity in Steam and Dry Methane Reforming over Nickel: Activity and Carbon Formation. ACS Catalysis, 2020, 10, 1428-1438.	5.5	109
128	1s2p Resonant Inelastic X-ray Scattering of Iron Oxides. Journal of Physical Chemistry B, 2005, 109, 20751-20762.	1.2	108
129	Diffuse Reflectance Spectroscopy of Supported Chromium Oxide Catalysts: A Self-Modeling Mixture Analysis. Journal of Catalysis, 1997, 166, 160-171.	3.1	106
130	A Combined SAXS/WAXS/XAFS Setup Capable of Observing Concurrent Changes Across the Nano-to-Micrometer Size Range in Inorganic Solid Crystallization Processes. Journal of the American Chemical Society, 2006, 128, 12386-12387.	6.6	106
131	In SituRaman Spectroscopy of Supported Chromium Oxide Catalysts:Â Reactivity Studies with Methanol and Butane. The Journal of Physical Chemistry, 1996, 100, 14437-14442.	2.9	105
132	Transition Metal Ions in Microporous Crystalline Aluminophosphates: Isomorphous Substitution. European Journal of Inorganic Chemistry, 1999, 1999, 565-577.	1.0	105
133	Nanoscale tomography reveals the deactivation of automotive copper-exchanged zeolite catalysts. Nature Communications, 2017, 8, 1666.	5.8	105
134	Bridging the Gap between the Direct and Hydrocarbon Pool Mechanisms of the Methanolâ€ŧoâ€Hydrocarbons Process. Angewandte Chemie - International Edition, 2018, 57, 8095-8099.	7.2	104
135	Propane to olefins tandem catalysis: a selective route towards light olefins production. Chemical Society Reviews, 2021, 50, 11503-11529.	18.7	104
136	Catalytic oxidation of aromatic oxygenates by the heterogeneous catalyst Co-ZIF-9. Applied Catalysis A: General, 2011, 394, 79-85.	2.2	103
137	Selective, one-pot catalytic conversion of levulinic acid to pentanoic acid over Ru/H-ZSM5. Journal of Catalysis, 2014, 320, 33-41.	3.1	103
138	Influence of the preparation method on the hydrotreating activity of MoS2/Al2O3 extrudates: A Raman microspectroscopy study on the genesis of the active phase. Journal of Catalysis, 2006, 243, 292-302.	3.1	102
139	Homogeneity of Titania-Silica Mixed Oxides: On UV-DRS Studies as a Function of Titania Content. Journal of Catalysis, 1996, 163, 489-491.	3.1	101
140	Supported Vanadium Oxide Catalysts: Quantitative Spectroscopy, Preferential Adsorption of V4+/5+, and Al2O3Coating of Zeolite Y. Journal of Physical Chemistry B, 1998, 102, 8005-8012.	1.2	101
141	Engineering the acidity and accessibility of the zeolite ZSM-5 for efficient bio-oil upgrading in catalytic pyrolysis of lignocellulose. Green Chemistry, 2018, 20, 3499-3511.	4.6	101
142	Transition metal-catalyzed oxidative double bond cleavage of simple and bio-derived alkenes and unsaturated fatty acids. Catalysis Science and Technology, 2014, 4, 2182.	2.1	99
143	Operando monitoring of temperature and active species at the single catalyst particle level. Nature Catalysis, 2019, 2, 986-996.	16.1	99
144	Redox Behavior and Dispersion of Supported Chromium Catalysts. The Journal of Physical Chemistry, 1995, 99, 320-326.	2.9	98

#	Article	IF	CITATIONS
145	In situ Raman spectroscopy studies of bulk and surface metal oxide phases during oxidation reactions. Catalysis Today, 1996, 32, 47-55.	2.2	98
146	Revealing Shape Selectivity and Catalytic Activity Trends Within the Pores of Hâ€ZSMâ€5 Crystals by Time― and Spaceâ€Resolved Optical and Fluorescence Microspectroscopy. Chemistry - A European Journal, 2007, 13, 7057-7065.	1.7	98
147	Selective adsorption of manganese onto cobalt for optimized Mn/Co/TiO2 Fischer–Tropsch catalysts. Journal of Catalysis, 2010, 270, 95-102.	3.1	98
148	Operando Raman spectroscopy study on the deactivation of Pt/Al2O3 and Pt–Sn/Al2O3 propane dehydrogenation catalysts. Physical Chemistry Chemical Physics, 2013, 15, 12095.	1.3	98
149	Dynamic Xâ€Ray Diffraction Computed Tomography Reveals Realâ€Time Insight into Catalyst Active Phase Evolution. Angewandte Chemie - International Edition, 2011, 50, 10148-10152.	7.2	97
150	Mapping Metals Incorporation of a Whole Single Catalyst Particle Using Element Specific X-ray Nanotomography. Journal of the American Chemical Society, 2015, 137, 102-105.	6.6	97
151	Tandem Catalytic Depolymerization of Lignin by Waterâ€Tolerant Lewis Acids and Rhodium Complexes. ChemSusChem, 2016, 9, 2074-2079.	3.6	97
152	Electron paramagnetic resonance of heterogeneous chromium catalysts. Journal of the Chemical Society, Faraday Transactions, 1996, 92, 2431.	1.7	96
153	The role of Cu on the reduction behavior and surface properties of Fe-based Fischer–Tropsch catalysts. Physical Chemistry Chemical Physics, 2010, 12, 667-680.	1.3	96
154	Oxidation of methane to methanol and formaldehyde over Co–ZSM-5 molecular sieves: Tuning the reactivity and selectivity by alkaline and acid treatments of the zeolite ZSM-5 agglomerates. Microporous and Mesoporous Materials, 2011, 138, 176-183.	2.2	96
155	Hard Xâ€ray Nanotomography of Catalytic Solids at Work. Angewandte Chemie - International Edition, 2012, 51, 11986-11990.	7.2	96
156	Reactivity Descriptor in Solid Acid Catalysis: Predicting Turnover Frequencies for Propene Methylation in Zeotypes. Journal of Physical Chemistry Letters, 2014, 5, 1516-1521.	2.1	96
157	Towards real-time spectroscopic process control for the dehydrogenation of propane over supported chromium oxide catalysts. Chemical Engineering Science, 2004, 59, 5487-5492.	1.9	95
158	Ex Situ and Operando Studies on the Role of Copper in Cu-Promoted SiO <sub>2</sub> –MgO Catalysts for the Lebedev Ethanol-to-Butadiene Process. ACS Catalysis, 2015, 5, 6005-6015.	5.5	95
159	Influence of the Reaction Temperature on the Nature of the Active and Deactivating Species During Methanol-to-Olefins Conversion over H-SAPO-34. ACS Catalysis, 2017, 7, 5268-5281.	5.5	95
160	Modeling the 2-His-1-Carboxylate Facial Triad:Â Ironâ^'Catecholato Complexes as Structural and Functional Models of the Extradiol Cleaving Dioxygenases. Journal of the American Chemical Society, 2007, 129, 2275-2286.	6.6	94
161	The Porosity, Acidity, and Reactivity of Dealuminated Zeolite ZSMâ€5 at the Single Particle Level: The Influence of the Zeolite Architecture. Chemistry - A European Journal, 2011, 17, 13773-13781.	1.7	94
162	Unlocking the potential of a sleeping giant: lignins as sustainable raw materials for renewable fuels, chemicals and materials. Green Chemistry, 2015, 17, 4860-4861.	4.6	91

#	Article	IF	CITATIONS
163	Nanoscale Chemical Imaging of an Individual Catalyst Particle with Soft X-ray Ptychography. ACS Catalysis, 2016, 6, 2178-2181.	5.5	91
164	In Situ Luminescence Thermometry To Locally Measure Temperature Gradients during Catalytic Reactions. ACS Catalysis, 2018, 8, 2397-2401.	5.5	91
165	Synthesis, Spectroscopy and Catalysis of [Cr(acac)3] Complexes Grafted onto MCM-41 Materials: Formation of Polyethylene Nanofibres within Mesoporous Crystalline Aluminosilicates. Chemistry - A European Journal, 2000, 6, 2960-2970.	1.7	90
166	In situ spectroscopic investigation of the cobalt-catalyzed oxidation of lignin model compounds in ionic liquids. Green Chemistry, 2011, 13, 671.	4.6	90
167	In Situ Synchrotronâ€Based IR Microspectroscopy To Study Catalytic Reactions in Zeolite Crystals. Angewandte Chemie - International Edition, 2008, 47, 3543-3547.	7.2	88
168	Partial Oxidation of Methane Over Co-ZSM-5: Tuning the Oxygenate Selectivity by Altering the Preparation Route. Catalysis Letters, 2010, 136, 52-56.	1.4	88
169	Cold on Different Manganese Oxides: Ultra-Low-Temperature CO Oxidation over Colloidal Gold Supported on Bulk-MnO <sub>2</sub> Nanomaterials. Journal of the American Chemical Society, 2016, 138, 9572-9580.	6.6	88
170	Isotherms of individual pores by gas adsorption crystallography. Nature Chemistry, 2019, 11, 562-570.	6.6	88
171	Nanoscale chemical imaging using tip-enhanced Raman spectroscopy. Nature Protocols, 2019, 14, 1169-1193.	5.5	86
172	Highâ€Resolution Singleâ€Molecule Fluorescence Imaging of Zeolite Aggregates within Realâ€Life Fluid Catalytic Cracking Particles. Angewandte Chemie - International Edition, 2015, 54, 1836-1840.	7.2	85
173	Real time quantitative Raman spectroscopy of supported metal oxide catalysts without the need of an internal standard. Physical Chemistry Chemical Physics, 2005, 7, 211.	1.3	82
174	On the Surface Chemistry of Iron Oxides in Reactive Gas Atmospheres. Angewandte Chemie - International Edition, 2011, 50, 1584-1588.	7.2	82
175	Stability of Pt/γ-Al <sub>2</sub> O <sub>3</sub> Catalysts in Lignin and Lignin Model Compound Solutions under Liquid Phase Reforming Reaction Conditions. ACS Catalysis, 2013, 3, 464-473.	5.5	82
176	Operando spectroscopic investigation of supported metal oxide catalysts by combined time-resolved UV-VIS/Raman/on-line mass spectrometry. Physical Chemistry Chemical Physics, 2003, 5, 4361-4365.	1.3	81
177	A Facile Solidâ€Phase Route to Renewable Aromatic Chemicals from Biobased Furanics. Angewandte Chemie - International Edition, 2016, 55, 1368-1371.	7.2	81
178	Spatially Resolved Raman and UV-visible-NIR Spectroscopy on the Preparation of Supported Catalyst Bodies: Controlling the Formation of H2PMo11CoO405â^ Inside Al2O3 Pellets During Impregnation. Chemistry - A European Journal, 2005, 11, 4591-4601.	1.7	80
179	Intergrowth Structure of Zeolite Crystals and Pore Orientation of Individual Subunits Revealed by Electron Backscatter Diffraction/Focused Ion Beam Experiments. Angewandte Chemie - International Edition, 2008, 47, 5637-5640.	7.2	80
180	Visualizing pore architecture and molecular transport boundaries in catalyst bodies with fluorescent nanoprobes. Nature Chemistry, 2019, 11, 23-31.	6.6	80

#	Article	IF	CITATIONS
181	In situ UV–Vis diffuse reflectance spectroscopy — on line activity measurements of supported chromium oxide catalysts: relating isobutane dehydrogenation activity with Cr-speciation via experimental design. Journal of Molecular Catalysis A, 2000, 151, 115-131.	4.8	79
182	H <sub>2</sub> Adsorption on 3d Transition Metal Clusters:  A Combined Infrared Spectroscopy and Density Functional Study. Journal of Physical Chemistry A, 2008, 112, 1139-1149.	1.1	79
183	Promoted cobalt metal catalysts suitable for the production of lower olefins from natural gas. Nature Communications, 2019, 10, 167.	5.8	79
184	New Insights into the Coordination Chemistry and Molecular Structure of Copper(II) Histidine Complexes in Aqueous Solutions. Inorganic Chemistry, 2006, 45, 1960-1971.	1.9	78
185	Plastic Waste Conversion over a Refinery Waste Catalyst. Angewandte Chemie - International Edition, 2021, 60, 16101-16108.	7.2	78
186	Synthesis and chemistry of chromium in CrAPO-5 molecular sieves. Zeolites, 1994, 14, 360-366.	0.9	77
187	Kβ-Detected XANES of Framework-Substituted FeZSM-5 Zeolites. Journal of Physical Chemistry B, 2004, 108, 10002-10011.	1.2	77
188	Geometry and Framework Interactions of Zeolite-Encapsulated Copper(II)â^'Histidine Complexes. Journal of the American Chemical Society, 2000, 122, 11488-11496.	6.6	76
189	Giant and explosive plasmonic bubbles by delayed nucleation. Proceedings of the National Academy of Sciences of the United States of America, 2018, 115, 7676-7681.	3.3	76
190	Unique Organicâ^'Inorganic Interactions Leading to a Structure-Directed Microporous Aluminophosphate Crystallization as Observed with in situ Raman Spectroscopy. Journal of the American Chemical Society, 2006, 128, 11744-11745.	6.6	75
191	Active sites over CuO/CeO2 and inverse CeO2/CuO catalysts for preferential CO oxidation. Journal of Power Sources, 2014, 256, 301-311.	4.0	75
192	Catalytic Conversion of Methane into Aromatic Hydrocarbons over Iron Oxide Loaded ZSM-5 Zeolites. Angewandte Chemie International Edition in English, 1997, 36, 2374-2376.	4.4	74
193	Promotion Effects in the Oxidation of CO over Zeolite-Supported Pt Nanoparticles. Journal of Physical Chemistry B, 2005, 109, 3822-3831.	1.2	74
194	Synchrotron Radiation Effects on Catalytic Systems As Probed with a Combined In-Situ UVâ^'Vis/XAFS Spectroscopic Setup. Journal of Physical Chemistry B, 2005, 109, 4042-4047.	1.2	74
195	Correlating Metal Poisoning with Zeolite Deactivation in an Individual Catalyst Particle by Chemical and Phase‣ensitive Xâ€ray Microscopy. Angewandte Chemie - International Edition, 2013, 52, 5983-5987.	7.2	74
196	Coke Formation in a Zeolite Crystal During the Methanolâ€ŧoâ€Hydrocarbons Reaction as Studied with Atom Probe Tomography. Angewandte Chemie - International Edition, 2016, 55, 11173-11177.	7.2	74
197	Relating structure and composition with accessibility of a single catalyst particle using correlative 3-dimensional micro-spectroscopy. Nature Communications, 2016, 7, 12634.	5.8	74
198	The Multifaceted Role of Methylaluminoxane in Metallocene-Based Olefin Polymerization Catalysis. Macromolecules, 2018, 51, 343-355.	2.2	74

#	Article	IF	CITATIONS
199	Active phase evolution in single Ni/Al <sub>2</sub> O <sub>3</sub> methanation catalyst bodies studied in real time using combined 14/4-XRD-CT and 14/4-absorption-CT. Chemical Science, 2012, 3, 509-523.	3.7	73
200	Oxygenated commodity chemicals from chemo atalytic conversion of biomass derived heterocycles. AICHE Journal, 2018, 64, 1910-1922.	1.8	73
201	Highly Selective Oxidation of Methane into Methanol over Cu-Promoted Monomeric Fe/ZSM-5. ACS Catalysis, 2021, 11, 6684-6691.	5.5	73
202	Destructive Adsorption of Carbon Tetrachloride on Alkaline Earth Metal Oxides. Journal of Physical Chemistry B, 1998, 102, 3773-3778.	1.2	72
203	Electron Spin Resonance of High-Spin Cobalt in Microporous Crystalline Cobalt-Containing Aluminophosphates. Journal of Physical Chemistry B, 2000, 104, 37-42.	1.2	72
204	Carboxylate Binding in Copper Histidine Complexes in Solution and in Zeolite Y:  X- and W-band Pulsed EPR/ENDOR Combined with DFT Calculations. Journal of the American Chemical Society, 2004, 126, 11733-11745.	6.6	72
205	Nanoscale Chemical Imaging of the Reduction Behavior of a Single Catalyst Particle. Angewandte Chemie - International Edition, 2009, 48, 3632-3636.	7.2	72
206	Methane-to-methanol conversion over zeolite Cu-SSZ-13, and its comparison with the selective catalytic reduction of NO <sub>x</sub> with NH <sub>3</sub> . Catalysis Science and Technology, 2018, 8, 1028-1038.	2.1	72
207	Multiscale Mechanistic Insights of Shaped Catalyst Body Formulations and Their Impact on Catalytic Properties. ACS Catalysis, 2019, 9, 4792-4803.	5.5	72
208	Zeolite-Encapsulated Copper(II) Amino Acid Complexes: Synthesis, Spectroscopy, and Catalysis. The Journal of Physical Chemistry, 1996, 100, 9456-9461.	2.9	71
209	X-ray nanoscopy of cobalt Fischer–Tropsch catalysts at work. Chemical Communications, 2013, 49, 4622.	2.2	71
210	Single Molecule Nanospectroscopy Visualizes Proton-Transfer Processes within a Zeolite Crystal. Journal of the American Chemical Society, 2016, 138, 13586-13596.	6.6	71
211	Suppression of the Aromatic Cycle in Methanolâ€toâ€Olefins Reaction over ZSMâ€5 by Postâ€Synthetic Modification Using Calcium. ChemCatChem, 2016, 8, 3057-3063.	1.8	71
212	Creating value from plastic waste. Science, 2020, 370, 400-401.	6.0	71
213	Spectroscopy, microscopy, diffraction and scattering of archetypal MOFs: formation, metal sites in catalysis and thin films. Chemical Society Reviews, 2020, 49, 6694-6732.	18.7	71
214	Vanadium-Incorporated MCM-48 Materials:Â Optimization of the Synthesis Procedure and an in Situ Spectroscopic Study of the Vanadium Species. Journal of Physical Chemistry B, 2001, 105, 3393-3399.	1.2	70
215	Mechanistic Studies on Chabaziteâ€Type Methanolâ€toâ€Olefin Catalysts: Insights from Timeâ€Resolved UV/Vis Microspectroscopy Combined with Theoretical Simulations. ChemCatChem, 2013, 5, 173-184.	1.8	70
216	Single-Molecule Fluorescence Microscopy Reveals Local Diffusion Coefficients in the Pore Network of an Individual Catalyst Particle. Journal of the American Chemical Society, 2017, 139, 13632-13635.	6.6	70

#	Article	IF	CITATIONS
217	Highly Active Catalysts for the Telomerization of Crude Glycerol with 1,3â€Butadiene. ChemSusChem, 2008, 1, 193-196.	3.6	69
218	Quantitative 3D Fluorescence Imaging of Single Catalytic Turnovers Reveals Spatiotemporal Gradients in Reactivity of Zeolite H-ZSM-5 Crystals upon Steaming. Journal of the American Chemical Society, 2015, 137, 6559-6568.	6.6	69
219	Hydrogenation of levulinic acid to γ-valerolactone over anatase-supported Ru catalysts: Effect of catalyst synthesis protocols on activity. Applied Catalysis A: General, 2018, 549, 197-206.	2.2	69
220	Electrophilic aromatic substitution over zeolites generates Wheland-type reaction intermediates. Nature Catalysis, 2018, 1, 23-31.	16.1	69
221	Deconvoluting the Competing Effects of Zeolite Framework Topology and Diffusion Path Length on Methanol to Hydrocarbons Reaction. ACS Catalysis, 2018, 8, 11042-11053.	5.5	69
222	Uncovering the reaction mechanism behind CoO as active phase for CO2 hydrogenation. Nature Communications, 2022, 13, 324.	5.8	69
223	Identification of Intermediates in Zeoliteâ€Catalyzed Reactions by In Situ UV/Vis Microspectroscopy and a Complementary Set of Molecular Simulations. Chemistry - A European Journal, 2013, 19, 16595-16606.	1.7	68
224	Nanoscale chemical imaging of solid–liquid interfaces using tip-enhanced Raman spectroscopy. Nanoscale, 2018, 10, 1815-1824.	2.8	68
225	Gallium-promoted HZSM-5 zeolites as efficient catalysts for the aromatization of biomass-derived furans. Chemical Engineering Science, 2019, 198, 305-316.	1.9	68
226	Binder Effects in SiO <sub>2</sub> ―and Al <sub>2</sub> O <sub>3</sub> â€Bound Zeolite ZSMâ€5â€Based Extrudates as Studied by Microspectroscopy. ChemCatChem, 2015, 7, 1312-1321.	1.8	67
227	CO <sub>2</sub> Hydrogenation over Pt-Containing UiO-67 Zr-MOFs—The Base Case. Industrial & Engineering Chemistry Research, 2017, 56, 13206-13218.	1.8	67
228	Mechanistic Insight in the Ethane Dehydrogenation Reaction over Cr/Al2O3 Catalysts. Catalysis Letters, 2005, 103, 143-148.	1.4	66
229	Role of Magnesium Silicates in Wet-Kneaded Silica–Magnesia Catalysts for the Lebedev Ethanol-to-Butadiene Process. ACS Catalysis, 2016, 6, 4034-4045.	5.5	66
230	Noninvasive In Situ Visualization of Supported Catalyst Preparations Using Multinuclear Magnetic Resonance Imaging. Journal of the American Chemical Society, 2005, 127, 11916-11917.	6.6	65
231	Effect of the Nickel Precursor on the Impregnation and Drying of γ-Al <sub>2</sub> O <sub>3</sub> Catalyst Bodies:  A UVâ^'vis and IR Microspectroscopic Study. Journal of Physical Chemistry C, 2008, 112, 7201-7209.	1.5	65
232	Labelâ€Free Chemical Imaging of Catalytic Solids by Coherent Antiâ€Stokes Raman Scattering and Synchrotronâ€Based Infrared Microscopy. Angewandte Chemie - International Edition, 2009, 48, 8990-8994.	7.2	65
233	Zeolites and Zeotypes for Oil and Gas Conversion. Advances in Catalysis, 2015, 58, 143-314.	0.1	65
234	Tandem catalysis with double-shelled hollow spheres. Nature Materials, 2022, 21, 572-579.	13.3	65

#	Article	IF	CITATIONS
235	In Situ Raman Spectroscopy of Supported Chromium Oxide Catalysts:  18O2â^'16O2 Isotopic Labeling Studies. Journal of Physical Chemistry B, 1997, 101, 2793-2796.	1.2	64
236	Phase Segregation in Ceriumâ^'Lanthanum Solid Solutions. Journal of Physical Chemistry B, 2006, 110, 9984-9990.	1.2	64
237	Enhanced Photoresponse of FeS <sub>2</sub> Films: The Role of Marcasite–Pyrite Phase Junctions. Advanced Materials, 2016, 28, 9602-9607.	11.1	64
238	Luminescence thermometry for <i>in situ</i> temperature measurements in microfluidic devices. Lab on A Chip, 2019, 19, 1236-1246.	3.1	64
239	Chemistry and spectroscopy of vanadium in VAPO-5 molecular sieves. Zeolites, 1995, 15, 482-489.	0.9	63
240	Combined EXAFS and STEM-EELS study of the electronic state and location of Mn as promoter in Co-based Fischer–Tropsch catalysts. Physical Chemistry Chemical Physics, 2005, 7, 568-572.	1.3	63
241	Architectureâ€Dependent Distribution of Mesopores in Steamed Zeolite Crystals as Visualized by FIB‧EM Tomography. Angewandte Chemie - International Edition, 2011, 50, 1294-1298.	7.2	63
242	Mechanistic Insights into the Oxidation of Veratryl Alcohol with Co(salen) and Oxygen in Aqueous Media: An in-situ Spectroscopic Study. European Journal of Inorganic Chemistry, 2005, 2005, 2591-2599.	1.0	62
243	Theoretical Study on the Role of Surface Basicity and Lewis Acidity on the Etherification of Glycerol over Alkaline Earth Metal Oxides. Chemistry - A European Journal, 2009, 15, 10864-10870.	1.7	62
244	Xâ€ray Imaging of Zeolite Particles at the Nanoscale: Influence of Steaming on the State of Aluminum and the Methanolâ€Toâ€Olefin Reaction. Angewandte Chemie - International Edition, 2012, 51, 3616-3619.	7.2	62
245	Substituted Phthalic Anhydrides from Biobased Furanics: A New Approach to Renewable Aromatics. ChemSusChem, 2015, 8, 3052-3056.	3.6	62
246	Xâ€ray Fluorescence Tomography of Aged Fluidâ€Catalyticâ€Cracking Catalyst Particles Reveals Insight into Metal Deposition Processes. ChemCatChem, 2015, 7, 3674-3682.	1.8	62
247	Combined Operando Xâ€ray Diffraction/Raman Spectroscopy of Catalytic Solids in the Laboratory: The Co/TiO <sub>2</sub> Fischer–Tropsch Synthesis Catalyst Showcase. ChemCatChem, 2016, 8, 1531-1542.	1.8	62
248	Decoding Nucleation and Growth of Zeolitic Imidazolate Framework Thin Films with Atomic Force Microscopy and Vibrational Spectroscopy. Chemistry - A European Journal, 2017, 23, 10915-10924.	1.7	62
249	Revealing Lattice Expansion of Small-Pore Zeolite Catalysts during the Methanol-to-Olefins Process Using Combined Operando X-ray Diffraction and UV–vis Spectroscopy. ACS Catalysis, 2018, 8, 2060-2070.	5.5	62
250	Die nÃ <b>e</b> hste Generation des Recyclings – neues Leben für Kunststoffmüll. Angewandte Chemie, 2020, 132, 15524-15548.	1.6	62
251	Raman spectroscopy of supported chromium oxide catalysts. Determination of chromium—oxygen bond distances and bond orders. Journal of the Chemical Society, Faraday Transactions, 1996, 92, 1969-1973.	1.7	61
252	Probing the Influence of X-rays on Aqueous Copper Solutions Using Time-Resolved in Situ Combined Video/X-ray Absorption Near-Edge/Ultravioletâ^Visible Spectroscopy. Journal of Physical Chemistry B, 2006, 110, 17671-17677.	1.2	61

#	Article	IF	CITATIONS
253	Guest–host interactions of arenes in H-ZSM-5 and their impact on methanol-to-hydrocarbons deactivation processes. Journal of Catalysis, 2013, 300, 235-241.	3.1	61
254	Full, Reactive Solubilization of Humin Byproducts by Alkaline Treatment and Characterization of the Alkali-Treated Humins Formed. ACS Sustainable Chemistry and Engineering, 2015, 3, 533-543.	3.2	61
255	The curious case of zeolite–clay/binder interactions and their consequences for catalyst preparation. Faraday Discussions, 2016, 188, 369-386.	1.6	61
256	<i>Operando</i> Nanoscale Sensors in Catalysis: All Eyes on Catalyst Particles. ACS Nano, 2020, 14, 3725-3735.	7.3	61
257	Supported Tantalum Oxide and Supported Vanadia-tantala Mixed Oxides: Structural Characterization and Surface Properties. Journal of Physical Chemistry B, 2001, 105, 6211-6220.	1.2	60
258	UVâ^'Vis Microspectroscopy:  Probing the Initial Stages of Supported Metal Oxide Catalyst Preparation. Journal of the American Chemical Society, 2005, 127, 5024-5025.	6.6	60
259	Zeolite Framework Stabilized Copper Complex Inspired by the 2-His-1-carboxylate Facial Triad Motif Yielding Oxidation Catalysts. Journal of the American Chemical Society, 2006, 128, 3208-3217.	6.6	60
260	In situ UV–VIS diffuse reflectance spectroscopy–on-line activity measurements Significance of Cr n+ species ( n=2, 3 and 6) in n-butane dehydrogenation catalyzed by supported chromium oxide catalysts. Journal of the Chemical Society, Faraday Transactions, 1998, 94, 2011-2014.	1.7	59
261	An iron molybdate catalyst for methanol to formaldehyde conversion prepared by a hydrothermal method and its characterization. Applied Catalysis A: General, 2009, 363, 143-152.	2.2	58
262	New Insights into the Active Surface Species of Silver Alumina Catalysts in the Selective Catalytic Reduction of NO. Journal of Physical Chemistry C, 2011, 115, 885-896.	1.5	58
263	Template–Framework Interactions in Tetraethylammoniumâ€Directed Zeolite Synthesis. Angewandte Chemie - International Edition, 2016, 55, 16044-16048.	7.2	58
264	Destructive adsorption of carbon tetrachloride on lanthanum and cerium oxides. Physical Chemistry Chemical Physics, 1999, 1, 3157-3162.	1.3	57
265	Tomographic Energy Dispersive Diffraction Imaging To Study the Genesis of Ni Nanoparticles in 3D within γ-Al <sub>2</sub> O <sub>3</sub> Catalyst Bodies. Journal of the American Chemical Society, 2009, 131, 16932-16938.	6.6	57
266	Dynamic Cu/Zn Interaction in SiO <sub>2</sub> Supported Methanol Synthesis Catalysts Unraveled by in Situ XAFS. Journal of Physical Chemistry C, 2011, 115, 20175-20191.	1.5	57
267	Combined Operando UV/Vis/IR Spectroscopy Reveals the Role of Methoxy and Aromatic Species during the Methanolâ€ŧoâ€Olefins Reaction over H‣APOâ€34. ChemCatChem, 2014, 6, 3396-3408.	1.8	57
268	Mechanistic Insights into Growth of Surfaceâ€Mounted Metalâ€Organic Framework Films Resolved by Infrared (Nanoâ€) Spectroscopy. Chemistry - A European Journal, 2018, 24, 187-195.	1.7	57
269	Catalytic Fast Pyrolysis of Biomass: Catalyst Characterization Reveals the Feed-Dependent Deactivation of a Technical ZSM-5-Based Catalyst. ACS Sustainable Chemistry and Engineering, 2021, 9, 291-304.	3.2	57
270	Mapping Elevated Temperatures with a Micrometer Resolution Using the Luminescence of Chemically Stable Upconversion Nanoparticles. ACS Applied Nano Materials, 2021, 4, 4208-4215.	2.4	57

#	Article	IF	CITATIONS
271	Zeolite Encaged Cu(Histidine) Complexes as Mimics of Natural Cu Enzymes. Angewandte Chemie International Edition in English, 1996, 34, 2652-2654.	4.4	56
272	Study of the coordination of Cu2+ in zeolite Y: Interaction with water and ammonia. Microporous and Mesoporous Materials, 2000, 37, 209-222.	2.2	56
273	Palladium-Based Telomerization of 1,3-Butadiene with Glycerol Using Methoxy-Functionalized Triphenylphosphine Ligands. Chemistry - A European Journal, 2008, 14, 8995-9005.	1.7	56
274	On the interaction between Co- and Mo-complexes in impregnation solutions used for the preparation of Al2O3-supported HDS catalysts: A combined Raman/UV–vis–NIR spectroscopy study. Catalysis Today, 2008, 130, 117-125.	2.2	56
275	Progress in controlling the size, composition and nanostructure of supported gold–palladium nanoparticles for catalytic applications. Catalysis Science and Technology, 2013, 3, 2869.	2.1	56
276	Initial Carbon–Carbon Bond Formation during the Early Stages of the Methanolâ€toâ€Olefin Process Proven by Zeoliteâ€Trapped Acetate and Methyl Acetate. Angewandte Chemie, 2016, 128, 16072-16077.	1.6	56
277	Effect of Mg and Zr Modification on the Activity of VOx/Al2O3 Catalysts in the Dehydrogenation of Butanes. Journal of Catalysis, 2001, 203, 242-252.	3.1	55
278	Modeling of kinetics and deactivation in the direct epoxidation of propene over gold–titania catalysts. Journal of Catalysis, 2005, 236, 153-163.	3.1	55
279	Chemical Imaging of Catalyst Deactivation during the Conversion of Renewables at the Single Particle Level: Etherification of Biomass-Based Polyols with Alkenes over H-Beta Zeolites. Journal of the American Chemical Society, 2010, 132, 10429-10439.	6.6	55
280	Surface- and Tip-Enhanced Raman Spectroscopy as Operando Probes for Monitoring and Understanding Heterogeneous Catalysis. Catalysis Letters, 2015, 145, 40-57.	1.4	55
281	Methanol-to-olefins process over zeolite catalysts with DDR topology: effect of composition and structural defects on catalytic performance. Catalysis Science and Technology, 2016, 6, 2663-2678.	2.1	55
282	Spatiotemporal coke formation over zeolite ZSM-5 during the methanol-to-olefins process as studied with <i>operando</i> UV-vis spectroscopy: a comparison between H-ZSM-5 and Mg-ZSM-5. Catalysis Science and Technology, 2018, 8, 1632-1644.	2.1	55
283	Surface chemistry of silica–titania-supported chromium oxide catalysts. Journal of the Chemical Society, Faraday Transactions, 1995, 91, 953-961.	1.7	54
284	In Situ Diffuse Reflectance Spectroscopy of Supported Chromium Oxide Catalysts:  Kinetics of the Reduction Process with Carbon Monoxide. Journal of Physical Chemistry B, 1997, 101, 2824-2829.	1.2	54
285	Singleâ€Particle Spectroscopy on Large SAPOâ€34 Crystals at Work: Methanolâ€ŧoâ€Olefin versus Ethanolâ€ŧoâ€Olefin Processes. Chemistry - A European Journal, 2013, 19, 11204-11215.	1.7	54
286	Aqueous-phase reforming of crude glycerol: effect of impurities on hydrogen production. Catalysis Science and Technology, 2016, 6, 134-143.	2.1	54
287	Low-Temperature Destruction of Chlorinated Hydrocarbons over Lanthanide Oxide Based Catalysts. Angewandte Chemie - International Edition, 2002, 41, 4730-4732.	7.2	53
288	Atomic XAFS as a Tool To Probe the Reactivity of Metal Oxide Catalysts:Â Quantifying Metal Oxide Support Effects. Journal of the American Chemical Society, 2007, 129, 3189-3197.	6.6	53

#	Article	lF	CITATIONS
289	Editorial Highlight: Molecules in confined spaces. Physical Chemistry Chemical Physics, 2009, 11, 2794.	1.3	53
290	Cooperative Role of Water Molecules during the Initial Stage of Water-Induced Zeolite Dealumination. ACS Catalysis, 2019, 9, 5119-5135.	5.5	53
291	Monitoring Chromia/Alumina Catalysts in Situ during Propane Dehydrogenation by Optical Fiber UV–Visible Diffuse Reflectance Spectroscopy. Journal of Catalysis, 2001, 204, 253-257.	3.1	52
292	Tomographic Energy Dispersive Diffraction Imaging as a Tool To Profile in Three Dimensions the Distribution and Composition of Metal Oxide Species in Catalyst Bodies. Angewandte Chemie - International Edition, 2007, 46, 8832-8835.	7.2	52
293	In Situ Nanoscale Investigation of Catalytic Reactions in the Liquid Phase Using Zirconia-Protected Tip-Enhanced Raman Spectroscopy Probes. Journal of Physical Chemistry Letters, 2019, 10, 1669-1675.	2.1	52
294	Spectroscopic evidence for the adsorption of propene on gold nanoparticles during the hydro-epoxidation of propene. Journal of Catalysis, 2008, 258, 256-264.	3.1	51
295	Combination of characterization techniques for atomic layer deposition MoO3 coatings: From the amorphous to the orthorhombic α-MoO3 crystalline phase. Journal of Vacuum Science and Technology A: Vacuum, Surfaces and Films, 2012, 30, .	0.9	51
296	Interplay between nanoscale reactivity and bulk performance of H-ZSM-5 catalysts during the methanol-to-hydrocarbons reaction. Journal of Catalysis, 2013, 307, 185-193.	3.1	51
297	Intergrowth Structure and Aluminium Zoning of a Zeolite ZSMâ€5 Crystal as Resolved by Synchrotronâ€Based Micro Xâ€Ray Diffraction Imaging. Angewandte Chemie - International Edition, 2013, 52, 13382-13386.	7.2	51
298	Hard Xâ€ray Spectroscopic Nanoâ€lmaging of Hierarchical Functional Materials at Work. ChemPhysChem, 2013, 14, 3655-3666.	1.0	51
299	Enhanced activity of desilicated Cu-SSZ-13 for the selective catalytic reduction of NO <sub>x</sub> and its comparison with steamed Cu-SSZ-13. Catalysis Science and Technology, 2017, 7, 3851-3862.	2.1	51
300	Ĵ›O4Upside Down:Â A New Molecular Structure for Supported VO4Catalysts. Journal of Physical Chemistry B, 2005, 109, 10223-10233.	1.2	50
301	Probing the Transport of Paramagnetic Complexes inside Catalyst Bodies in a Quantitative Manner by Magnetic Resonance Imaging. Angewandte Chemie - International Edition, 2007, 46, 7224-7227.	7.2	50
302	Monitoring Transport Phenomena of Paramagnetic Metalâ€Ion Complexes Inside Catalyst Bodies with Magnetic Resonance Imaging. Chemistry - A European Journal, 2008, 14, 2363-2374.	1.7	50
303	Operando UV-Vis spectroscopy of a catalytic solid in a pilot-scale reactor: deactivation of a CrOx/Al2O3 propane dehydrogenation catalyst. Chemical Communications, 2013, 49, 1518.	2.2	50
304	Single-catalyst particle spectroscopy of alcohol-to-olefins conversions: Comparison between SAPO-34 and SSZ-13. Catalysis Today, 2014, 226, 14-24.	2.2	50
305	Iridium-catalysed primary alcohol oxidation and hydrogen shuttling for the depolymerisation of lignin. Green Chemistry, 2018, 20, 3214-3221.	4.6	50
306	Range-extended EXAFS at theLedge of rare earths using high-energy-resolution fluorescence detection: A study of La in LaOCI. Physical Review B, 2005, 72, .	1.1	49

#	Article	IF	CITATIONS
307	Hexane Cracking over Steamed Phosphated Zeolite Hâ€ZSMâ€5: Promotional Effect on Catalyst Performance and Stability. Chemistry - A European Journal, 2014, 20, 16922-16932.	1.7	49
308	Thermally Stable and Regenerable Platinum–Tin Clusters for Propane Dehydrogenation Prepared by Atom Trapping on Ceria. Angewandte Chemie, 2017, 129, 9114-9119.	1.6	49
309	Chemically and thermally stable lanthanide-doped Y2O3 nanoparticles for remote temperature sensing in catalytic environments. Chemical Engineering Science, 2019, 198, 235-240.	1.9	49
310	Disentangling Reaction Processes of Zeolites within Singleâ€Oriented Channels. Angewandte Chemie - International Edition, 2020, 59, 15502-15506.	7.2	49
311	Identifying key mononuclear Fe species for low-temperature methane oxidation. Chemical Science, 2021, 12, 3152-3160.	3.7	49
312	The effect of nutrient supplementation on the biofiltration removal of butanal in contaminated air. Applied Microbiology and Biotechnology, 1993, 39, 395.	1.7	48
313	Synthesis and characterization of alumina-supported vanadium oxide catalysts prepared by the molecular designed dispersion of VO(acac)2 complexes. Physical Chemistry Chemical Physics, 2000, 2, 2673-2680.	1.3	48
314	A new model for the molecular structure of supported vanadium oxide catalysts. Chemical Physics Letters, 2004, 397, 277-281.	1.2	48
315	Molecular Structure of a Supported VO4Cluster and Its Interfacial Geometry as a Function of the SiO2, Nb2O5, and ZrO2Support. Journal of Physical Chemistry B, 2006, 110, 14313-14325.	1.2	48
316	Synthesis of long alkyl chain ethers through direct etherification of biomass-based alcohols with 1-octene over heterogeneous acid catalysts. Journal of Catalysis, 2009, 268, 251-259.	3.1	48
317	Local silico-aluminophosphate interfaces within phosphated H-ZSM-5 zeolites. Physical Chemistry Chemical Physics, 2014, 16, 9892.	1.3	48
318	Integrated Transmission Electron and Singleâ€Molecule Fluorescence Microscopy Correlates Reactivity with Ultrastructure in a Single Catalyst Particle. Angewandte Chemie - International Edition, 2018, 57, 257-261.	7.2	48
319	Core–shell H-ZSM-5/silicalite-1 composites: BrÃ,nsted acidity and catalyst deactivation at the individual particle level. Physical Chemistry Chemical Physics, 2011, 13, 15985.	1.3	47
320	Effects of Coke Deposits on the Catalytic Performance of Large Zeolite Hâ€ZSMâ€5 Crystals during Alcoholâ€ŧoâ€Hydrocarbon Reactions as Investigated by a Combination of Optical Spectroscopy and Microscopy. Chemistry - A European Journal, 2015, 21, 17324-17335.	1.7	47
321	Influence of Sulfuric Acid on the Performance of Rutheniumâ€based Catalysts in the Liquidâ€Phase Hydrogenation of Levulinic Acid to γâ€Valerolactone. ChemSusChem, 2017, 10, 2891-2896.	3.6	47
322	Chemical targets to deactivate biological and chemical toxins using surfaces and fabrics. Nature Reviews Chemistry, 2021, 5, 370-387.	13.8	47
323	Diffuse Reflectance Spectroscopy of Dehydrated Cobalt-Exchanged Faujasite-Type Zeolites: A New Method for Co2+ Siting. The Journal of Physical Chemistry, 1995, 99, 15222-15228.	2.9	46
324	Spectroscopic characterization of an MoOx layer on the surface of silica. An evaluation of the molecular designed dispersion method. Physical Chemistry Chemical Physics, 1999, 1, 4099-4104.	1.3	46

#	Article	IF	CITATIONS
325	Relating Structure and Chemical Composition with Lewis Acidity in Zeolites:Â A Spectroscopic Study with Probe Molecules. Journal of Physical Chemistry B, 2001, 105, 4904-4911.	1.2	46
326	The siting of Cu(II) in mordenite: a theoretical spectroscopic study. Physical Chemistry Chemical Physics, 2002, 4, 134-145.	1.3	46
327	Solid Acidâ€Catalyzed Cellulose Hydrolysis Monitored by Inâ€Situ ATRâ€IR Spectroscopy. ChemSusChem, 2012, 5, 430-437.	' 3.6	46
328	Integrated Laser and Electron Microscopy Correlates Structure of Fluid Catalytic Cracking Particles to BrA,nsted Acidity. Angewandte Chemie - International Edition, 2012, 51, 1428-1431.	7.2	45
329	FIB-SEM Tomography Probes the Mesoscale Pore Space of an Individual Catalytic Cracking Particle. ACS Catalysis, 2016, 6, 3158-3167.	5.5	45
330	Simultaneous coking and dealumination of zeolite H-ZSM-5 during the transformation of chloromethane into olefins. Catalysis Science and Technology, 2016, 6, 296-306.	2.1	45
331	Characterization of deactivated and regenerated zeolite ZSM-5-based catalyst extrudates used in catalytic pyrolysis of biomass. Journal of Catalysis, 2019, 380, 108-122.	3.1	45
332	ESR Fine Structure of Manganese lons in Zeolite A Detects Strong Variations of the Coordination Environment. Journal of the American Chemical Society, 1996, 118, 9615-9622.	6.6	44
333	Single-site heterogeneous Cr-based catalyst for the selective trimerisation of ethylene. Chemical Communications, 2005, , 1865.	2.2	44
334	Telomerization of 1,3-butadiene with various alcohols by Pd/TOMPP catalysts: new opportunities for catalytic biomass valorization. Green Chemistry, 2009, 11, 1155.	4.6	44
335	Fe atalyzed Oneâ€Pot Oxidative Cleavage of Unsaturated Fatty Acids into Aldehydes with Hydrogen Peroxide and Sodium Periodate. Chemistry - A European Journal, 2013, 19, 15012-15018.	1.7	44
336	Phosphatation of Zeolite Hâ€ZSMâ€5: A Combined Microscopy and Spectroscopy Study. ChemPhysChem, 2014, 15, 283-292.	1.0	44
337	Agglutination of single catalyst particles during fluid catalytic cracking as observed by X-ray nanotomography. Chemical Communications, 2015, 51, 8097-8100.	2.2	44
338	Thermally Stable TiO <sub>2</sub> ―and SiO <sub>2</sub> â€5hellâ€Isolated Au Nanoparticles for In Situ Plasmonâ€Enhanced Raman Spectroscopy of Hydrogenation Catalysts. Chemistry - A European Journal, 2018, 24, 3733-3741.	1.7	44
339	Combined In Situ X-ray Powder Diffractometry/Raman Spectroscopy of Iron Carbide and Carbon Species Evolution in Fe(â~`Na–S)/α-Al <sub>2</sub> O <sub>3</sub> Catalysts during Fischer–Tropsch Synthesis. ACS Catalysis, 2020, 10, 9837-9855.	5.5	44
340	Bis(μ-oxo)dicopper as Key Intermediate in the Catalytic Decomposition of Nitric Oxide. ChemPhysChem, 2003, 4, 626-630.	1.0	43
341	New frontiers in X-ray spectroscopy in heterogeneous catalysis: Using Fe/ZSM-5 as test-system. Catalysis Today, 2005, 110, 228-238.	2.2	43
342	Hydrogen-Induced Transition from Dissociative to Molecular Chemisorption of CO on Vanadium Clusters. Journal of the American Chemical Society, 2007, 129, 2516-2520.	6.6	43

#	Article	IF	CITATIONS
343	The role of synchrotron radiation in examining the self-assembly of crystalline nanoporous framework materials: from zeolites and aluminophosphates to metal organic hybrids. Chemical Society Reviews, 2010, 39, 4767.	18.7	43
344	Staining of Fluid atalytic racking Catalysts: Localising BrÃ,nsted Acidity within a Single Catalyst Particle. Chemistry - A European Journal, 2012, 18, 1094-1101.	1.7	43
345	In situ spectroscopic investigation of oxidative dehydrogenation and disproportionation of benzyl alcohol. Physical Chemistry Chemical Physics, 2013, 15, 12147.	1.3	43
346	Realâ€Time Quantitative Operando Raman Spectroscopy of a CrO <sub>x</sub> /Al <sub>2</sub> O <sub>3</sub> Propane Dehydrogenation Catalyst in a Pilot‣cale Reactor. ChemCatChem, 2014, 6, 3139-3145.	1.8	43
347	Active phase distribution changes within a catalyst particle during Fischer–Tropsch synthesis as revealed by multi-scale microscopy. Catalysis Science and Technology, 2016, 6, 4438-4449.	2.1	43
348	Probing acid sites in solid catalysts with pyridine UV-Vis spectroscopy. Physical Chemistry Chemical Physics, 2018, 20, 21647-21659.	1.3	43
349	Geminal Diol of Dihydrolevoglucosenone as a Switchable Hydrotrope: A Continuum of Green Nanostructured Solvents. ACS Sustainable Chemistry and Engineering, 2019, 7, 7878-7883.	3.2	43
350	Zeoliteâ€Tailored Active Site Proximity for the Efficient Production of Pentanoic Biofuels. Angewandte Chemie - International Edition, 2021, 60, 23713-23721.	7.2	43
351	Styrene oligomerization as a molecular probe reaction for zeolite acidity: a UV-Vis spectroscopy and DFT study. Physical Chemistry Chemical Physics, 2010, 12, 7032.	1.3	42
352	Visualizing Dealumination of a Single Zeolite Domain in a Realâ€Life Catalytic Cracking Particle. Angewandte Chemie - International Edition, 2016, 55, 11134-11138.	7.2	42
353	Capturing the Genesis of an Active Fischer–Tropsch Synthesis Catalyst with Operando Xâ€ray Nanospectroscopy. Angewandte Chemie - International Edition, 2018, 57, 11957-11962.	7.2	42
354	Chemistry and Spectroscopy of Chromium in Zeolites. Studies in Surface Science and Catalysis, 1994, 84, 965-972.	1.5	41
355	In-Situ Soft X-ray Absorption of Over-exchanged Fe/ZSM5. Journal of Physical Chemistry B, 2003, 107, 13069-13075.	1.2	41
356	Experimental and theoretical IR study of methanol and ethanol conversion over H-SAPO-34. Catalysis Today, 2011, 177, 12-24.	2.2	41
357	Homogeneous and heterogenised masked N-heterocyclic carbenes for bio-based cyclic carbonate synthesis. Green Chemistry, 2016, 18, 1605-1618.	4.6	41
358	<i>In Situ</i> Local Temperature Mapping in Microscopy Nanoâ€Reactors with Luminescence Thermometry. ChemCatChem, 2019, 11, 5505-5512.	1.8	41
359	Correlated X-ray Ptychography and Fluorescence Nano-Tomography on the Fragmentation Behavior of an Individual Catalyst Particle during the Early Stages of Olefin Polymerization. Journal of the American Chemical Society, 2020, 142, 3691-3695.	6.6	41
360	Low-Temperature Destruction of Carbon Tetrachloride over Lanthanide Oxide-Based Catalysts: From Destructive Adsorption to a Catalytic Reaction Cycle. Chemistry - A European Journal, 2004, 10, 1637-1646.	1.7	40

#	Article	IF	CITATIONS
361	Die Schiefergasrevolution: eine Chance zur Herstellung von Chemikalien auf Biobasis?. Angewandte Chemie, 2013, 125, 12198-12206.	1.6	40
362	Highly Oriented Growth of Catalytically Active Zeolite ZSMâ€5 Films with a Broad Range of Si/Al Ratios. Angewandte Chemie - International Edition, 2017, 56, 11217-11221.	7.2	40
363	Atomic XAFS as a Tool to Probe the Electronic Properties of Supported Noble Metal Nanoclusters. Journal of the American Chemical Society, 2005, 127, 3272-3273.	6.6	39
364	Host–Guest Chemistry of Copper(II)–Histidine Complexes Encaged in Zeolite Y. Chemistry - A European Journal, 2006, 12, 7167-7177.	1.7	39
365	The Effect of Charge on CO Binding in Rhodium Carbonyls:  From Bridging to Terminal CO. Journal of the American Chemical Society, 2008, 130, 2126-2127.	6.6	39
366	Magnetic Resonance Imaging Studies on Catalyst Impregnation Processes: Discriminating Metal Ion Complexes within Millimeter-Sized γ-Al <sub>2</sub> O <sub>3</sub> Catalyst Bodies. Journal of the American Chemical Society, 2009, 131, 6525-6534.	6.6	39
367	On the Active Oxygen in Bulk MoO3 during the Anaerobic Dehydrogenation of Methanol. Journal of Physical Chemistry C, 2009, 113, 4890-4897.	1.5	39
368	Alkaline treatment of template containing zeolites: Introducing mesoporosity while preserving acidity. Catalysis Today, 2011, 168, 48-56.	2.2	39
369	Supported bimetallic nano-alloys as highly active catalysts for the one-pot tandem synthesis of imines and secondary amines from nitrobenzene and alcohols. Catalysis Science and Technology, 2016, 6, 5473-5482.	2.1	39
370	The active phase in cobalt-based Fischer-Tropsch synthesis. Chem Catalysis, 2021, 1, 339-363.	2.9	39
371	Insights into the Preparation of Supported Catalysts:Â A Spatially Resolved Raman and UVâ^'Vis Spectroscopic Study into the Drying Process of CoMo/γ-Al2O3Catalyst Bodies. Journal of Physical Chemistry B, 2005, 109, 14513-14522.	1.2	38
372	The Interpretation of Sulfur K-Edge XANES Spectra: A Case Study on Thiophenic and Aliphatic Sulfur Compounds. Journal of Physical Chemistry A, 2009, 113, 2750-2756.	1.1	38
373	Spatial Distribution of Zeolite ZSMâ€5 within Catalyst Bodies Affects Selectivity and Stability of Methanolâ€ŧoâ€Hydrocarbons Conversion. ChemCatChem, 2013, 5, 2827-2831.	1.8	38
374	Unraveling the Homologation Reaction Sequence of the Zeoliteâ€Catalyzed Ethanolâ€ŧoâ€Hydrocarbons Process. Angewandte Chemie - International Edition, 2019, 58, 3908-3912.	7.2	38
375	Unusual Coordination Behavior of Cr3+in Microporous Aluminophosphates. Journal of Physical Chemistry B, 2006, 110, 716-722.	1.2	37
376	Development of a 4,4′-biphenyl/phosphine-based COF for the heterogeneous Pd-catalysed telomerisation of 1,3-butadiene. Catalysis Science and Technology, 2013, 3, 2571.	2.1	37
377	Molybdenum Speciation and its Impact on Catalytic Activity during Methane Dehydroaromatization in Zeolite ZSMâ€5 as Revealed by Operando Xâ€Ray Methods. Angewandte Chemie, 2016, 128, 5301-5305.	1.6	37
378	Electrolyte Effects on the Stability of Niâ^'Mo Cathodes for the Hydrogen Evolution Reaction. ChemSusChem, 2019, 12, 3491-3500.	3.6	37

#	Article	IF	CITATIONS
379	Recovery and conversion of acetic acid from a phosphonium phosphinate ionic liquid to enable valorization of fermented wastewater. Green Chemistry, 2019, 21, 2023-2034.	4.6	37
380	Enhanced Catalytic Performance through In Situ Encapsulation of Ultrafine Ru Clusters within a High-Aluminum Zeolite. ACS Catalysis, 2022, 12, 1847-1856.	5.5	37
381	Baseâ€free Pd/TOMPPâ€Catalyzed Telomerization of 1,3â€Butadiene with Carbohydrates and Sugar Alcohols. ChemSusChem, 2009, 2, 855-858.	3.6	36
382	Controlled Synthesis of Phaseâ€Pure Zeolitic Imidazolate Framework Coâ€ZIFâ€9. European Journal of Inorganic Chemistry, 2015, 2015, 1625-1630.	1.0	36
383	Fluoride-assisted synthesis of bimodal microporous SSZ-13 zeolite. Chemical Communications, 2016, 52, 3227-3230.	2.2	36
384	Increasing the availability of active sites in Zn-Co double metal cyanides by dispersion onto a SiO2 support. Journal of Catalysis, 2017, 354, 92-99.	3.1	36
385	Nickel Poisoning of a Cracking Catalyst Unravelled by Singleâ€Particle Xâ€ray Fluorescenceâ€Diffractionâ€Absorption Tomography. Angewandte Chemie - International Edition, 2020, 59, 3922-3927.	7.2	36
386	Real-Time Control of a Catalytic Solid in a Fixed-Bed Reactor Based on In Situ Spectroscopy. Angewandte Chemie - International Edition, 2007, 46, 5412-5416.	7.2	35
387	Profiling Physicochemical Changes within Catalyst Bodies during Preparation: New Insights from Invasive and Noninvasive Microspectroscopic Studies. Accounts of Chemical Research, 2010, 43, 1279-1288.	7.6	35
388	Probing ZnAPO-34 Self-Assembly Using Simultaneous Multiple in Situ Techniques. Journal of Physical Chemistry C, 2011, 115, 6331-6340.	1.5	35
389	Chemical imaging of the sulfur-induced deactivation of Cu/ZnO catalyst bodies. Journal of Catalysis, 2014, 314, 94-100.	3.1	35
390	Extending the plasmonic lifetime of tip-enhanced Raman spectroscopy probes. Physical Chemistry Chemical Physics, 2016, 18, 13710-13716.	1.3	35
391	Catalytic Hydrogenation of Renewable Levulinic Acid to γ-Valerolactone: Insights into the Influence of Feed Impurities on Catalyst Performance in Batch and Flow Reactors. ACS Sustainable Chemistry and Engineering, 2020, 8, 5903-5919.	3.2	35
392	Low-temperature catalytic destruction of CCl4, CHCl3 and CH2Cl2 over basic oxides. Physical Chemistry Chemical Physics, 2004, 6, 5256.	1.3	34
393	Relative Activity of La2O3, LaOCl, and LaCl3 in Reaction with CCl4 Studied with Infrared Spectroscopy and Density Functional Theory Calculations. Journal of Physical Chemistry B, 2005, 109, 11634-11642.	1.2	34
394	Destructive Adsorption of CCl4over Lanthanum-Based Solids:Â Linking Activity to Acidâ^'Base Properties. Journal of Physical Chemistry B, 2005, 109, 23993-24001.	1.2	34
395	The role of support oxygen in the epoxidation of propene over gold–titania catalysts investigated by isotopic transient kinetics. Journal of Catalysis, 2009, 265, 161-169.	3.1	34
396	On the Synergistic Catalytic Properties of Bimetallic Mesoporous Materials Containing Aluminum and Zirconium: The Prins Cyclisation of Citronellal. Chemistry - A European Journal, 2011, 17, 2077-2088.	1.7	34

#	Article	IF	CITATIONS
397	Closing the operando gap: The application of high energy photons for studying catalytic solids at work. Applied Catalysis A: General, 2011, 391, 468-476.	2.2	34
398	Microspectroscopic insight into the deactivation process of individual cracking catalyst particles with basic sulfur components. Applied Catalysis A: General, 2012, 419-420, 84-94.	2.2	34
399	Highly Selective Bimetallic Ptâ€Cu/Mg(Al)O Catalysts for the Aqueousâ€Phase Reforming of Glycerol. ChemCatChem, 2013, 5, 529-537.	1.8	34
400	Differences in the Location of Guest Molecules within Zeolite Pores As Revealed by Multilaser Excitation Confocal Fluorescence Microscopy: Which Molecule Is Where?. Journal of the American Chemical Society, 2015, 137, 1916-1928.	6.6	34
401	Zeolite molecular accessibility and host–guest interactions studied by adsorption of organic probes of tunable size. Physical Chemistry Chemical Physics, 2017, 19, 1857-1867.	1.3	34
402	Deactivation of Cuâ€Exchanged Automotiveâ€Emission NH <sub>3</sub> â€SCR Catalysts Elucidated with Nanoscale Resolution Using Scanning Transmission Xâ€ray Microscopy. Angewandte Chemie - International Edition, 2020, 59, 15610-15617.	7.2	34
403	3D Nanoscale Chemical Imaging of the Distribution of Aluminum Coordination Environments in Zeolites with Soft Xâ€Ray Microscopy. ChemPhysChem, 2013, 14, 496-499.	1.0	33
404	Aluminum-Phosphate Binder Formation in Zeolites as Probed with X-ray Absorption Microscopy. Journal of the American Chemical Society, 2014, 136, 17774-17787.	6.6	33
405	Fe(6-Me-PyTACN)-catalyzed, one-pot oxidative cleavage of methyl oleate and oleic acid into carboxylic acids with H2O2 and NaIO4. Catalysis Science and Technology, 2014, 4, 708.	2.1	33
406	Quantification and Classification of Carbonyls in Industrial Humins and Lignins by <sup>19</sup> F NMR. ACS Sustainable Chemistry and Engineering, 2017, 5, 965-972.	3.2	33
407	On the Cobalt Carbide Formation in a Co/TiO <sub>2</sub> Fischer–Tropsch Synthesis Catalyst as Studied by High-Pressure, Long-Term <i>Operando</i> X-ray Absorption and Diffraction. ACS Catalysis, 2021, 11, 2956-2967.	5.5	33
408	Electron crystallography with the EIGER detector. IUCrJ, 2018, 5, 190-199.	1.0	33
409	Dynamic restructuring of supported metal nanoparticles and its implications for structure insensitive catalysis. Nature Communications, 2021, 12, 7096.	5.8	33
410	Bis(1-methylimidazol-2-yl)propionates and Bis(1-methylbenzimidazol-2-yl)-propionates: A New Family of BiomimeticN,N,OLigands - Synthesis, Structures and Cull Coordination Complexes. European Journal of Inorganic Chemistry, 2005, 2005, 779-787.	1.0	32
411	New insight in the template decomposition process of large zeolite ZSM-5 crystals: an in situUV-Vis/fluorescence micro-spectroscopy study. Physical Chemistry Chemical Physics, 2011, 13, 3681-3685.	1.3	32
412	Xâ€Ray Imaging of SAPOâ€34 Molecular Sieves at the Nanoscale: Influence of Steaming on the Methanolâ€ŧoâ€Hydrocarbons Reaction. ChemCatChem, 2013, 5, 1386-1394.	1.8	32
413	Probing the Different Life Stages of a Fluid Catalytic Cracking Particle with Integrated Laser and Electron Microscopy. Chemistry - A European Journal, 2013, 19, 3846-3859.	1.7	32
414	Silica deposition as an approach for improving the hydrothermal stability of an alumina support during glycerol aqueous phase reforming. Applied Catalysis A: General, 2018, 551, 13-22.	2.2	32

#	Article	IF	CITATIONS
415	Microfluidics and catalyst particles. Lab on A Chip, 2019, 19, 3575-3601.	3.1	32
416	<i>In Situ</i> Shell-Isolated Nanoparticle-Enhanced Raman Spectroscopy to Unravel Sequential Hydrogenation of Phenylacetylene over Platinum Nanoparticles. ACS Catalysis, 2019, 9, 10794-10802.	5.5	32
417	A quantitative diffuse reflectance spectroscopy study of chromium-containing zeolites. Zeolites, 1994, 14, 450-457.	0.9	31
418	Methanol oxidation over supported vanadium oxide catalysts: New fundamental insights about oxidation reactions over metal oxide catalysts from transient and steady state kinetics. Studies in Surface Science and Catalysis, 1997, , 305-314.	1.5	31
419	Dealing with a local heating effect when measuring catalytic solids in a reactor with Raman spectroscopy. Physical Chemistry Chemical Physics, 2006, 8, 2413.	1.3	31
420	An integrated AFM-Raman instrument for studying heterogeneous catalytic systems: a first showcase. Chemical Communications, 2012, 48, 1742.	2.2	31
421	Skeletal isomerisation of oleic acid over ferrierite in the presence and absence of triphenylphosphine: Pore mouth catalysis and related deactivation mechanisms. Journal of Catalysis, 2014, 316, 24-35.	3.1	31
422	Polyethylene with Reverse Coâ€monomer Incorporation: From an Industrial Serendipitous Discovery to Fundamental Understanding. Angewandte Chemie - International Edition, 2015, 54, 13073-13079.	7.2	31
423	Visualizing Dealumination of a Single Zeolite Domain in a Realâ€Life Catalytic Cracking Particle. Angewandte Chemie, 2016, 128, 11300-11304.	1.6	31
424	Nanoscale Chemical Imaging of Zeolites Using Atom Probe Tomography. Angewandte Chemie - International Edition, 2018, 57, 10422-10435.	7.2	31
425	Deactivation of Sn-Beta during carbohydrate conversion. Applied Catalysis A: General, 2018, 564, 113-122.	2.2	31
426	Formation and Functioning of Bimetallic Nanocatalysts: The Power of Xâ€ray Probes. Angewandte Chemie - International Edition, 2019, 58, 13220-13230.	7.2	31
427	Cobalt nanocrystals on carbon nanotubes in the Fischer-Tropsch synthesis: Impact of support oxidation. Applied Catalysis A: General, 2020, 593, 117441.	2.2	31
428	Toward an e-chemistree: Materials for electrification of the chemical industry. MRS Bulletin, 2021, 46, 1187-1196.	1.7	31
429	Partial least squares modeling of combined infrared, 1H NMR and 13C NMR spectra to predict long residue properties of crude oils. Vibrational Spectroscopy, 2009, 51, 205-212.	1.2	30
430	On the Polymerization Behavior of Telomers: Metathesis versus Thiol–Ene Chemistry. Macromolecules, 2012, 45, 1866-1878.	2.2	30
431	Effect of Feedstock and Catalyst Impurities on the Methanolâ€toâ€Olefin Reaction over Hâ€SAPOâ€34. ChemCatChem, 2017, 9, 183-194.	1.8	30
432	<i>Inâ€situ</i> Xâ€Ray Absorption Near Edge Structure Spectroscopy of a Solid Catalyst using a Laboratoryâ€Based Setâ€up. ChemCatChem, 2019, 11, 1039-1044.	1.8	30

#	Article	IF	CITATIONS
433	Elucidating Zeolite Channel Geometry–Reaction Intermediate Relationships for the Methanolâ€ŧoâ€Hydrocarbon Process. Angewandte Chemie - International Edition, 2020, 59, 20024-20030.	7.2	30
434	Single-molecule observation of diffusion and catalysis in nanoporous solids. Adsorption, 2021, 27, 423-452.	1.4	30
435	Single Trap States in Single CdSe Nanoplatelets. ACS Nano, 2021, 15, 7216-7225.	7.3	30
436	Highly Mixed Phases in Ball-milled Cu/ZnO Catalysts:  An EXAFS and XANES Study. Journal of Physical Chemistry B, 2006, 110, 16892-16901.	1.2	29
437	Spatiotemporal Multitechnique Imaging of a Catalytic Solid in Action: Phase Variation and Volatilization During Molybdenum Oxide Reduction. ChemCatChem, 2009, 1, 99-102.	1.8	29
438	Facile Access to Key Reactive Intermediates in the Pd/PR <sub>3</sub> atalyzed Telomerization of 1,3â€Butadiene. Angewandte Chemie - International Edition, 2010, 49, 7972-7975.	7.2	29
439	A UV-Vis micro-spectroscopic study to rationalize the influence of Clâ^'(aq) on the formation of different Pd macro-distributions on l³-Al <sub>2</sub> O <sub>3</sub> catalyst bodies. Physical Chemistry Chemical Physics, 2010, 12, 97-107.	1.3	29
440	Large Zeolite Hâ€ZSMâ€5 Crystals as Models for the Methanolâ€toâ€Hydrocarbons Process: Bridging the Gap between Singleâ€Particle Examination and Bulk Catalyst Analysis. Chemistry - A European Journal, 2013, 19, 8533-8542.	1.7	29
441	A Facile Solidâ€Phase Route to Renewable Aromatic Chemicals from Biobased Furanics. Angewandte Chemie, 2016, 128, 1390-1393.	1.6	29
442	Operando Spectroscopy of the Gas-Phase Aldol Condensation of Propanal over Solid Base Catalysts. Topics in Catalysis, 2017, 60, 1522-1536.	1.3	29
443	Metalâ€Organic Frameworks as Catalyst Supports: Influence of Lattice Disorder on Metal Nanoparticle Formation. Chemistry - A European Journal, 2018, 24, 7498-7506.	1.7	29
444	Ethylene Polymerization over Metal–Organic Framework Crystallites and the Influence of Linkers on Their Fracturing Process. ACS Catalysis, 2019, 9, 3059-3069.	5.5	29
445	Insights into the activation of silica-supported metallocene olefin polymerization catalysts by methylaluminoxane. Catalysis Today, 2019, 334, 223-230.	2.2	29
446	Role of Rare Earth Ions in the Prevention of Dealumination of Zeolite Y for Fluid Cracking Catalysts. Journal of Physical Chemistry C, 2020, 124, 4626-4636.	1.5	29
447	<i>In situ</i> Nanoscale Infrared Spectroscopy of Water Adsorption on Nanoislands of Surfaceâ€Anchored Metalâ€Organic Frameworks. Angewandte Chemie - International Edition, 2021, 60, 1620-1624.	7.2	29
448	Water–active site interactions in zeolites and their relevance in catalysis. Trends in Chemistry, 2021, 3, 456-468.	4.4	29
449	Stabilization effects in binary colloidal Cu and Ag nanoparticle electrodes under electrochemical CO <sub>2</sub> reduction conditions. Nanoscale, 2021, 13, 4835-4844.	2.8	29
450	Monitoring the coordination of aluminium during microporous oxide crystallisation by in situ soft X-ray absorption spectroscopy. Chemical Communications, 2006, , 4410.	2.2	28

#	Article	IF	CITATIONS
451	Understanding the effect of postsynthesis ammonium treatment on the catalytic activity of Au/Ti-SBA-15 catalysts for the oxidation of propene. Journal of Catalysis, 2008, 259, 43-53.	3.1	28
452	Synthesis of octyl-ethers of biomass-based glycols through two competitive catalytic routes: Telomerization and etherification. Catalysis Today, 2010, 158, 130-138.	2.2	28
453	Clay intercalated Cu(II) amino acid complexes: synthesis, spectroscopy and catalysis. Clay Minerals, 1996, 31, 491-500.	0.2	27
454	Mobility of chromium in inorganic oxides Spectroscopic fingerprinting of oxidation states and coordination environments. Journal of the Chemical Society, Faraday Transactions, 1997, 93, 2117-2120.	1.7	27
455	Redox behaviour of over-exchanged Fe/ZSM5 zeolites studied with in-situ soft X-ray absorption spectroscopy. Physical Chemistry Chemical Physics, 2003, 5, 4484-4491.	1.3	27
456	The role of water in the epoxidation over gold–titania catalysts. Chemical Communications, 2005, , 6002.	2.2	27
457	Controlled Assembly of a Heterogeneous Single-Site Ethylene Trimerization Catalyst as Probed by X-ray Absorption Spectroscopy. Chemistry - A European Journal, 2006, 12, 4756-4763.	1.7	27
458	Selective Oxidation of Methanol to Hydrogen over Gold Catalysts Promoted by Alkalineâ€Earthâ€Metal and Lanthanum Oxides. ChemSusChem, 2009, 2, 743-748.	3.6	27
459	The Catalytic Conversion of Thiophenes over Large Hâ€ZSMâ€5 Crystals: An Xâ€Ray, UV/Vis, and Fluorescence Microspectroscopic Study. ChemCatChem, 2010, 2, 564-571.	1.8	27
460	Host–Guest Geometry in Pores of Zeolite ZSMâ€5 Spatially Resolved with Multiplex CARS Spectromicroscopy. Angewandte Chemie - International Edition, 2012, 51, 1343-1347.	7.2	27
461	Singleâ€Particle Spectroscopy of Alcoholâ€toâ€Olefins over SAPOâ€34 at Different Reaction Stages: Crystal Accessibility and Hydrocarbons Reactivity. ChemCatChem, 2014, 6, 772-783.	1.8	27
462	Large Ferrierite Crystals as Models for Catalyst Deactivation during Skeletal Isomerisation of Oleic Acid: Evidence for Pore Mouth Catalysis. Chemistry - A European Journal, 2016, 22, 199-210.	1.7	27
463	Spectroscopic study on the active site of a SiO <sub>2</sub> supported niobia catalyst used for the gas-phase Beckmann rearrangement of cyclohexanone oxime to ε-caprolactam. Physical Chemistry Chemical Physics, 2016, 18, 22636-22646.	1.3	27
464	A DNP-supported solid-state NMR study of carbon species in fluid catalytic cracking catalysts. Chemical Communications, 2017, 53, 3933-3936.	2.2	27
465	Isolating Clusters of Light Elements in Molecular Sieves with Atom Probe Tomography. Journal of the American Chemical Society, 2018, 140, 9154-9158.	6.6	27
466	Carbon Pathways, Sodiumâ€5ulphur Promotion and Identification of Iron Carbides in Ironâ€based Fischerâ€Tropsch Synthesis. ChemCatChem, 2020, 12, 4202-4223.	1.8	27
467	Hydrothermal synthesis of Co-rich CoAPO-5 molecular sieves. Physical Chemistry Chemical Physics, 2001, 3, 3240-3246.	1.3	26
468	Synthesis, characterization and catalysis of (Co, V)-, (Co, Cr)- and (Cr, V)APO-5 molecular sieves. Microporous and Mesoporous Materials, 2006, 94, 348-357.	2.2	26

#	Article	IF	CITATIONS
469	Dichloromethane as a Selective Modifying Agent To Create a Family of Highly Reactive Chromium Polymerization Sites. Angewandte Chemie - International Edition, 2007, 46, 1465-1468.	7.2	26
470	Geometric and Electronic Structure of α-Oxygen Sites in Mn-ZSM-5 Zeolites. Journal of Physical Chemistry C, 2008, 112, 12409-12416.	1.5	26
471	Detection of Carbocationic Species in Zeolites: Large Crystals Pave the Way. Chemistry - A European Journal, 2010, 16, 9340-9348.	1.7	26
472	Investigation of the Kinetics of a Surface Photocatalytic Reaction in Two Dimensions with Surface $\hat{a} \in e$ nhanced Raman Scattering. ChemCatChem, 2014, 6, 3342-3346.	1.8	26
473	Time-Resolved In Situ Liquid-Phase Atomic Force Microscopy and Infrared Nanospectroscopy during the Formation of Metal–Organic Framework Thin Films. Journal of Physical Chemistry Letters, 2018, 9, 1838-1844.	2.1	26
474	Direct observation of the electronic states of photoexcited hematite with ultrafast 2p3d X-ray absorption spectroscopy and resonant inelastic X-ray scattering. Physical Chemistry Chemical Physics, 2020, 22, 2685-2692.	1.3	26
475	Magnetic resonance imaging as an emerging tool for studying the preparation of supported catalysts. Applied Catalysis A: General, 2010, 374, 126-136.	2.2	25
476	Studying birth, life and death of catalytic solids with operando spectroscopy. National Science Review, 2015, 2, 147-149.	4.6	25
477	Nanoscale infrared imaging of zeolites using photoinduced force microscopy. Chemical Communications, 2017, 53, 13012-13014.	2.2	25
478	Incorporation of Transition Metal Ions in Aluminophosphate Molecular Sieves with AST Structure. Journal of Physical Chemistry B, 2001, 105, 2677-2686.	1.2	24
479	The Effect of Chemical Composition and Structure on XPS Binding Energies in Zeolites. Journal of Physical Chemistry B, 2003, 107, 678-684.	1.2	24
480	Manganese promotion in cobalt-based Fischer-Tropsch catalysis. Studies in Surface Science and Catalysis, 2004, 147, 271-276.	1.5	24
481	Cyclohexene Epoxidation with Cyclohexyl Hydroperoxide: A Catalytic Route to Largely Increase Oxygenate Yield from Cyclohexane Oxidation. ACS Catalysis, 2011, 1, 1183-1192.	5.5	24
482	Dispersion and Orientation of Zeolite ZSMâ€5 Crystallites within a Fluid Catalytic Cracking Catalyst Particle. Chemistry - A European Journal, 2014, 20, 3667-3677.	1.7	24
483	Skeletal isomerisation of oleic acid over ferrierite: Influence of acid site number, accessibility and strength on activity and selectivity. Journal of Catalysis, 2015, 329, 195-205.	3.1	24
484	Probing Zeolite Crystal Architecture and Structural Imperfections using Differently Sized Fluorescent Organic Probe Molecules. Chemistry - A European Journal, 2017, 23, 6305-6314.	1.7	24
485	Phaseâ€Dependent Stability and Substrateâ€Induced Deactivation by Strong Metalâ€Support Interaction of Ru/TiO <sub>2</sub> Catalysts for the Hydrogenation of Levulinic Acid. ChemCatChem, 2019, 11, 2079-2088.	1.8	24
486	<i>In Situ</i> X-ray Raman Scattering Spectroscopy of the Formation of Cobalt Carbides in a Co/TiO <sub>2</sub> Fischer–Tropsch Synthesis Catalyst. ACS Catalysis, 2021, 11, 809-819.	5.5	24

#	Article	IF	CITATIONS
487	Nature of adsorbed species during the reduction of CrO3/SiO2with CO In situFTIR spectroscopic study. Journal of the Chemical Society, Faraday Transactions, 1997, 93, 4065-4069.	1.7	23
488	On the synthesis of CoAPO-46, -11 and -44 molecular sieves from a Co(Ac)2·4H2O·Al(iPrO)3·H3PO4·Pr2NH·H2O gel via experimental design. Microporous and Mesoporous Materials, 1999, 27, 75-86.	2.2	23
489	Prediction of Long and Short Residue Properties of Crude Oils from Their Infrared and Near-Infrared Spectra. Applied Spectroscopy, 2008, 62, 414-422.	1.2	23
490	Promotion Effects in the Oxidation of CO over Zeolite-Supported Rh Nanoparticles. Journal of Physical Chemistry C, 2008, 112, 9394-9404.	1.5	23
491	Unified Internal Architecture and Surface Barriers for Molecular Diffusion of Microporous Crystalline Aluminophosphates. Angewandte Chemie - International Edition, 2010, 49, 6790-6794.	7.2	23
492	Chemical Probing within Catalyst Bodies by Diagonal Offset Raman Spectroscopy. Angewandte Chemie - International Edition, 2012, 51, 957-960.	7.2	23
493	Noninvasive Spatiotemporal Profiling of the Processes of Impregnation and Drying within Mo/Al <sub>2</sub> O <sub>3</sub> Catalyst Bodies by a Combination of X-ray Absorption Tomography and Diagonal Offset Raman Spectroscopy. ACS Catalysis, 2013, 3, 339-347.	5.5	23
494	Structure and acidity of individual Fluid Catalytic Cracking catalyst particles studied by synchrotron-based infrared micro-spectroscopy. Microporous and Mesoporous Materials, 2013, 166, 86-92.	2.2	23
495	Spatially-Resolved Photoluminescence of Monolayer MoS <sub>2</sub> under Controlled Environment for Ambient Optoelectronic Applications. ACS Applied Nano Materials, 2018, 1, 6226-6235.	2.4	23
496	High-throughput activity screening and sorting of single catalyst particles with a droplet microreactor using dielectrophoresis. Nature Catalysis, 2021, 4, 1070-1079.	16.1	23
497	Catalysts live and up close. Nature, 2006, 439, 548-548.	13.7	22
498	Dehydrochlorination of Intermediates in the Production of Vinyl Chloride over Lanthanum Oxide-Based Catalysts. Catalysis Letters, 2008, 122, 238-246.	1.4	22
499	Molecular adsorption of H2 on small cationic nickel clusters. Physical Chemistry Chemical Physics, 2008, 10, 5743.	1.3	22
500	Sulfur Speciation of Crude Oils by Partial Least Squares Regression Modeling of Their Infrared Spectra. Energy & Fuels, 2010, 24, 557-562.	2.5	22
501	Tracing Catalytic Conversion on Single Zeolite Crystals in 3D with Nonlinear Spectromicroscopy. Journal of the American Chemical Society, 2012, 134, 1124-1129.	6.6	22
502	A metal-free, one-pot method for the oxidative cleavage of internal aliphatic alkenes into carboxylic acids. RSC Advances, 2013, 3, 6606.	1.7	22
503	Experimental and Computational Evidence for the Mechanism of Intradiol Catechol Dioxygenation by Nonâ€Heme Iron(III) Complexes. Chemistry - A European Journal, 2014, 20, 15686-15691.	1.7	22
504	1s3p Resonant Inelastic X-ray Scattering of Cobalt Oxides and Sulfides. Journal of Physical Chemistry C, 2016, 120, 24063-24069.	1.5	22

#	Article	IF	CITATIONS
505	Reversible and Site-Dependent Proton-Transfer in Zeolites Uncovered at the Single-Molecule Level. Journal of the American Chemical Society, 2018, 140, 14195-14205.	6.6	22
506	3â€Ð Xâ€ray Nanotomography Reveals Different Carbon Deposition Mechanisms in a Single Catalyst Particle. ChemCatChem, 2021, 13, 2494-2507.	1.8	22
507	Catalytic Hydrogenâ€Chlorine Exchange between Chlorinated Hydrocarbons under Oxygenâ€Free Conditions. Angewandte Chemie - International Edition, 2008, 47, 5002-5004.	7.2	21
508	Catch me if you can!. Nature Chemistry, 2009, 1, 690-692.	6.6	21
509	Scanning Transmission Xâ€Ray Microscopy as a Novel Tool to Probe Colloidal and Photonic Crystals. Small, 2011, 7, 804-811.	5.2	21
510	Selectivity Control in the Tandem Aromatization of Bioâ€Based Furanics Catalyzed by Solid Acids and Palladium. ChemSusChem, 2017, 10, 277-286.	3.6	21
511	Probing the dynamics of photogenerated holes in doped hematite photoanodes for solar water splitting using transient absorption spectroscopy. Physical Chemistry Chemical Physics, 2018, 20, 9806-9811.	1.3	21
512	Catalytic production of hexane-1,2,5,6-tetrol from bio-renewable levoglucosanol in water: effect of metal and acid sites on (stereo)-selectivity. Green Chemistry, 2018, 20, 4557-4565.	4.6	21
513	3D Raman Spectroscopy of Large Zeolite ZSMâ€5 Crystals. Chemistry - A European Journal, 2019, 25, 7158-7167.	1.7	21
514	<i>Inâ€Situ</i> Shellâ€Isolated Nanoparticleâ€Enhanced Raman Spectroscopy of Nickelâ€Catalyzed Hydrogenation Reactions. ChemPhysChem, 2020, 21, 625-632.	1.0	21
515	Calcination temperature effects on Pd/alumina catalysts: Particle size, surface species and activity in methane combustion. Catalysis Today, 2021, 382, 120-129.	2.2	21
516	Solvent effects in the synthesis of CoAPO-5, -11 and -34 molecular sieves. Microporous and Mesoporous Materials, 2005, 84, 116-126.	2.2	20
517	Pore curvature and support composition effects on the electronic properties of supported Pt catalysts: An infrared spectroscopy study with CO as probe molecule. Vibrational Spectroscopy, 2008, 48, 92-100.	1.2	20
518	Functional Groups and Sulfur K-Edge XANES Spectra: Divalent Sulfur and Disulfides. Journal of Physical Chemistry A, 2010, 114, 9523-9528.	1.1	20
519	Operando surface spectroscopy—placing catalytic solids at work under the spotlight. Physical Chemistry Chemical Physics, 2012, 14, 2125.	1.3	20
520	Styrene oligomerization as a molecular probe reaction for BrÃ,nsted acidity at the nanoscale. Physical Chemistry Chemical Physics, 2012, 14, 6967.	1.3	20
521	Selective staining of BrÃ,nsted acidity in zeolite ZSM-5-based catalyst extrudates using thiophene as a probe. Physical Chemistry Chemical Physics, 2014, 16, 21531-21542.	1.3	20
522	Realâ€ŧime Analysis of a Working Triethylaluminiumâ€Modified Cr/Ti/SiO <sub>2</sub> Ethylene Polymerization Catalyst with Inâ€Situ Infrared Spectroscopy. ChemCatChem, 2016, 8, 1937-1944.	1.8	20

#	Article	IF	CITATIONS
523	Structure–performance relationships of Cr/Ti/SiO <sub>2</sub> catalysts modified with TEAl for oligomerisation of ethylene: tuning the selectivity towards 1-hexene. Catalysis Science and Technology, 2016, 6, 731-743.	2.1	20
524	Oxygen Vacancies in Reduced Rh/ and Pt/Ceria for Highly Selective and Reactive Reduction of NO into N <sub>2</sub> in excess of O <sub>2</sub> . ChemCatChem, 2017, 9, 2935-2938.	1.8	20
525	<i>Operando</i> micro-spectroscopy on ZSM-5 containing extrudates during the oligomerization of 1-hexene. Catalysis Science and Technology, 2018, 8, 2175-2185.	2.1	20
526	Toward Catalytic Ketonization of Volatile Fatty Acids Extracted from Fermented Wastewater by Adsorption. ACS Sustainable Chemistry and Engineering, 2020, 8, 11292-11298.	3.2	20
527	Heterogeneity in the Fragmentation of Ziegler Catalyst Particles during Ethylene Polymerization Quantified by X-ray Nanotomography. Jacs Au, 2021, 1, 852-864.	3.6	20
528	On the synthesis of vanadium containing molecular sieves by experimental design from a VOSO4÷5H2O·Al(iPrO)3·Pr2NH·H2O gel: occurrence of VAPO-41 as a secondary structure in the synthesis of VAPO-11. Microporous and Mesoporous Materials, 2000, 39, 493-507.	2.2	19
529	Promotion Effects in the Reduction of NO by CO over Zeolite-Supported Rh Catalysts. Journal of Physical Chemistry C, 2010, 114, 2282-2292.	1.5	19
530	Pd/TOMPP-catalysed telomerisation of 1,3-butadiene with lignin-type phenols and thermal Claisen rearrangement of linear telomers. Catalysis Science and Technology, 2013, 3, 1215-1223.	2.1	19
531	Imaging the effect of a hydrothermal treatment on the pore accessibility and acidity of large ZSM-5 zeolite crystals by selective staining. Catalysis Science and Technology, 2013, 3, 1208-1214.	2.1	19
532	Separation of Timeâ€Resolved Phenomena in Surfaceâ€Enhanced Raman Scattering of the Photocatalytic Reduction of <i>p</i> â€Nitrothiophenol. ChemPhysChem, 2015, 16, 547-554.	1.0	19
533	Uniformly Oriented Zeolite ZSMâ€5 Membranes with Tunable Wettability on a Porous Ceramic. Angewandte Chemie - International Edition, 2018, 57, 12458-12462.	7.2	19
534	Nanoscale Chemical Imaging of a Single Catalyst Particle with Tipâ€Enhanced Fluorescence Microscopy. ChemCatChem, 2019, 11, 417-423.	1.8	19
535	Probing the Location and Speciation of Elements in Zeolites with Correlated Atom Probe Tomography and Scanning Transmission Xâ€Ray Microscopy. ChemCatChem, 2019, 11, 488-494.	1.8	19
536	Matrix Effects in a Fluid Catalytic Cracking Catalyst Particle: Influence on Structure, Acidity, and Accessibility. Chemistry - A European Journal, 2020, 26, 11995-12009.	1.7	19
537	Unravelling Channel Structure–Diffusivity Relationships in Zeolite ZSMâ€5 at the Singleâ€Molecule Level. Angewandte Chemie - International Edition, 2022, 61, .	7.2	19
538	Spectroscopic characterization of supported Cr and Cr, Ti catalysts: Interaction with probe molecules. Studies in Surface Science and Catalysis, 1995, 91, 151-158.	1.5	18
539	Scaffolded amino acids as a close structural mimic of type-3 copper binding sites. Chemical Communications, 2007, , 4895.	2.2	18
540	Intermediates in the Destruction of Chlorinated C <sub>1</sub> Hydrocarbons on Laâ€Based Materials: Mechanistic Implications. Chemistry - A European Journal, 2007, 13, 9561-9571.	1.7	18

#	Article	IF	CITATIONS
541	Controlling the Bonding of CO on Cobalt Clusters by Coadsorption of H2. Angewandte Chemie - International Edition, 2007, 46, 5317-5320.	7.2	18
542	Telomerization of 1,3-Butadiene with Biomass-Derived Alcohols over a Heterogeneous Pd/TPPTS Catalyst Based on Layered Double Hydroxides. ACS Catalysis, 2011, 1, 526-536.	5.5	18
543	Spatial and temporal mapping of coke formation during paraffin and olefin aromatization in individual H-ZSM-5 crystals. Applied Catalysis A: General, 2011, 404, 12-20.	2.2	18
544	Mechanistic insights in the olefin epoxidation with cyclohexyl hydroperoxide. Catalysis Science and Technology, 2012, 2, 951.	2.1	18
545	Selective staining of zeolite acidity: Recent progress and future perspectives on fluorescence microscopy. Microporous and Mesoporous Materials, 2014, 189, 136-143.	2.2	18
546	Recent advances in secondary ion mass spectrometry of solid acid catalysts: large zeolite crystals under bombardment. Physical Chemistry Chemical Physics, 2014, 16, 5465-5474.	1.3	18
547	Practical Guidelines for Shellâ€Isolated Nanoparticleâ€Enhanced Raman Spectroscopy of Heterogeneous Catalysts. ChemPhysChem, 2018, 19, 2461-2467.	1.0	18
548	Magnetophoretic Sorting of Single Catalyst Particles. Angewandte Chemie - International Edition, 2018, 57, 10589-10594.	7.2	18
549	Revealing long- and short-range structural modifications within phosphorus-treated HZSM-5 zeolites by atom probe tomography, nuclear magnetic resonance and powder X-ray diffraction. Physical Chemistry Chemical Physics, 2018, 20, 27766-27777.	1.3	18
550	Catalytic hydrogenation of dihydrolevoglucosenone to levoglucosanol with a hydrotalcite/mixed oxide copper catalyst. Green Chemistry, 2019, 21, 5000-5007.	4.6	18
551	Charting a course for chemistry. Nature Chemistry, 2019, 11, 286-294.	6.6	18
552	Stable niobia-supported nickel catalysts for the hydrogenation of carbon monoxide to hydrocarbons. Catalysis Today, 2020, 343, 56-62.	2.2	18
553	Detection of Spontaneous FeOOH Formation at the Hematite/Ni(Fe)OOH Interface During Photoelectrochemical Water Splitting by Operando X-ray Absorption Spectroscopy. ACS Catalysis, 2021, 11, 12324-12335.	5.5	18
554	Synthesis and spectroscopy of clay intercalated Cu(II) bio-monomer complexes: coordination of Cu(II) with purines and nucleotides. Physical Chemistry Chemical Physics, 1999, 1, 2875-2880.	1.3	17
555	A Combined Multi-Technique In Situ Approach Used to Probe the Stability of Iron Molybdate Catalysts During Redox Cycling. Topics in Catalysis, 2009, 52, 1400-1409.	1.3	17
556	Mechanistic Study of the Pd/TOMPPâ€Catalyzed Telomerization of 1,3â€Butadiene with Biomassâ€Based Alcohols: On the Reversibility of Phosphine Alkylation. ChemCatChem, 2011, 3, 845-852.	1.8	17
557	Differences in single and aggregated nanoparticle plasmon spectroscopy. Physical Chemistry Chemical Physics, 2015, 17, 2991-2995.	1.3	17
558	Protonated thiophene-based oligomers as formed within zeolites: understanding their electron delocalization and aromaticity. Physical Chemistry Chemical Physics, 2016, 18, 2080-2086.	1.3	17

#	Article	IF	CITATIONS
559	Intra―and Interparticle Heterogeneities in Solid Activators for Singleâ€Site Olefin Polymerization Catalysis as Revealed by Microâ€Spectroscopy. Chemistry - A European Journal, 2018, 24, 11944-11953.	1.7	17
560	Bridging the Gap between the Direct and Hydrocarbon Pool Mechanisms of the Methanolâ€ŧoâ€Hydrocarbons Process. Angewandte Chemie, 2018, 130, 8227-8231.	1.6	17
561	Chemical Imaging of the Binderâ€Dependent Coke Formation in Zeoliteâ€Based Catalyst Bodies During the Transalkylation of Aromatics. ChemCatChem, 2019, 11, 4788-4796.	1.8	17
562	Template-Free Nanostructured Fluorine-Doped Tin Oxide Scaffolds for Photoelectrochemical Water Splitting. ACS Applied Materials & Interfaces, 2019, 11, 36485-36496.	4.0	17
563	Vibrational Fingerprinting of Defects Sites in Thin Films of Zeolitic Imidazolate Frameworks. Chemistry - A European Journal, 2019, 25, 8070-8084.	1.7	17
564	Scalingâ€Up of Bioâ€Oil Upgrading during Biomass Pyrolysis over ZrO <sub>2</sub> /ZSMâ€5â€Attapulgite. ChemSusChem, 2019, 12, 2428-2438.	3.6	17
565	Alkali Promotion in the Formation of CH <sub>4</sub> from CO <sub>2</sub> and Renewably Produced H <sub>2</sub> over Supported Ni Catalysts. ChemCatChem, 2020, 12, 2792-2800.	1.8	17
566	Early-stage particle fragmentation behavior of a commercial silica-supported metallocene catalyst. Catalysis Science and Technology, 2021, 11, 5335-5348.	2.1	17
567	Subâ€Second Timeâ€Resolved Surfaceâ€Enhanced Raman Spectroscopy Reveals Dynamic CO Intermediates during Electrochemical CO <sub>2</sub> Reduction on Copper. Angewandte Chemie, 2021, 133, 16712-16720.	1.6	17
568	Mechanistic Characterization of Zeolite-Catalyzed Aromatic Electrophilic Substitution at Realistic Operating Conditions. Jacs Au, 2022, 2, 502-514.	3.6	17
569	Coke Formation in a Zeolite Crystal During the Methanolâ€ŧoâ€Hydrocarbons Reaction as Studied with Atom Probe Tomography. Angewandte Chemie, 2016, 128, 11339-11343.	1.6	16
570	Genesis of MgCl <sub>2</sub> â€based Zieglerâ€Natta Catalysts as Probed with Operando Spectroscopy. ChemPhysChem, 2018, 19, 2662-2671.	1.0	16
571	Suzukiâ€Miyaura Cross oupling Using Plasmonic Pdâ€Decorated Au Nanorods as Catalyst: A Study on the Contribution of Laser Illumination. ChemCatChem, 2019, 11, 4974-4980.	1.8	16
572	Impact of Niobium in the Metal–Organic Framework-Mediated Synthesis of Co-Based Catalysts for Synthesis Gas Conversion. Catalysis Letters, 2019, 149, 3279-3286.	1.4	16
573	Elucidating the Kâ€Edge Xâ€Ray Absorption Nearâ€Edge Structure of Cobalt Carbide. ChemCatChem, 2019, 11, 3042-3045.	1.8	16
574	Melamineâ€Based Microporous Organic Framework Thin Films on an Alumina Membrane for Highâ€Flux Organic Solvent Nanofiltration. ChemSusChem, 2020, 13, 136-140.	3.6	16
575	Effect of Mesoporosity, Acidity and Crystal Size of Zeolite ZSMâ€5 on Catalytic Performance during the Exâ€situ Catalytic Fast Pyrolysis of Biomass. ChemCatChem, 2021, 13, 1207-1219.	1.8	16
576	Unravelling the effect of impurities on the methanol-to-olefins process in waste-derived zeolites ZSM-5. Journal of Catalysis, 2021, 396, 136-147.	3.1	16

#	Article	IF	CITATIONS
577	Efficient Synthesis of Monomeric Fe Species in Zeolite ZSMâ€5 for the Lowâ€Temperature Oxidation of Methane. ChemCatChem, 2021, 13, 2766-2770.	1.8	16
578	Structureâ€Activity Relationships in Highly Active Platinumâ€ī in MFlâ€ŧype Zeolite Catalysts for Propane Dehydrogenation. ChemCatChem, 2022, 14, .	1.8	16
579	Ethylene polymerization over chromium complexes grafted onto MCM-41 materials. Chemical Communications, 1999, , 445-446.	2.2	15
580	AlOxCoating of Ultrastable Zeolite Y:Â A Possible Method for Vanadium Passivation of FCC Catalysts. Journal of Physical Chemistry B, 2000, 104, 9195-9202.	1.2	15
581	Operando spectroscopy: fundamental and technical aspects of spectroscopy of catalysts under working conditions. Physical Chemistry Chemical Physics, 2003, 5, 1.	1.3	15
582	Influence of Levulinic Acid Hydrogenation on Aluminum Coordination in Zeolite‣upported Ruthenium Catalysts: A <sup>27</sup> Al 3QMAS Nuclear Magnetic Resonance Study. ChemPhysChem, 2018, 19, 379-385.	1.0	15
583	Quality control for Ziegler-Natta catalysis via spectroscopic fingerprinting. Journal of Catalysis, 2018, 363, 128-135.	3.1	15
584	Kinetics of Lifetime Changes in Bimetallic Nanocatalysts Revealed by Quick Xâ€ray Absorption Spectroscopy. Angewandte Chemie - International Edition, 2018, 57, 12430-12434.	7.2	15
585	Micro-spectroscopy of HKUST-1 metal–organic framework crystals loaded with tetracyanoquinodimethane: effects of water on host–guest chemistry and electrical conductivity. Physical Chemistry Chemical Physics, 2019, 21, 25678-25689.	1.3	15
586	Tandem catalytic aromatization of volatile fatty acids. Green Chemistry, 2020, 22, 3229-3238.	4.6	15
587	Crystal Phase Effects on the Gasâ€Phase Ketonization of Small Carboxylic Acids over TiO <sub>2</sub> Catalysts. ChemSusChem, 2021, 14, 2710-2720.	3.6	15
588	Correlating the Morphological Evolution of Individual Catalyst Particles to the Kinetic Behavior of Metallocene-Based Ethylene Polymerization Catalysts. Jacs Au, 2021, 1, 1996-2008.	3.6	15
589	Plugged Hexagonal Mesoporous Templated Silica : A unique micro- and mesoporous material with internal silica nanocapsules Studies in Surface Science and Catalysis, 2002, 141, 45-52.	1.5	14
590	Elucidation of the molecular structure of hydrated vanadium oxide species by X-ray absorption spectroscopy: correlation between the Vâ‹ V coordination number and distance and the point of zero charge of the support oxide. Physical Chemistry Chemical Physics, 2006, 8, 4814-4824.	1.3	14
591	Prediction of Long-Residue Properties of Potential Blends from Mathematically Mixed Infrared Spectra of Pure Crude Oils by Partial Least-Squares Regression Models. Energy & Fuels, 2009, 23, 2164-2168.	2.5	14
592	Chemical Reactivity Indices as a Tool for Understanding the Support-Effect in Supported Metal Oxide Catalysts. Journal of Physical Chemistry C, 2009, 113, 19905-19912.	1.5	14
593	Optical Investigation of the Intergrowth Structure and Accessibility of BrÃ,nsted Acid Sites in Etched SSZ-13 Zeolite Crystals by Confocal Fluorescence Microscopyâ€. Langmuir, 2010, 26, 16510-16516.	1.6	14
594	Catalytic oxidative cleavage of catechol by a non-heme iron(iii) complex as a green route to dimethyl adipate. Chemical Communications, 2013, 49, 6912.	2.2	14

#	Article	IF	CITATIONS
595	Reusable Mg–Al hydrotalcites for the catalytic synthesis of diglycerol dicarbonate from diglycerol and dimethyl carbonate. Catalysis Today, 2015, 257, 274-280.	2.2	14
596	Xâ€ray Excited Optical Fluorescence and Diffraction Imaging of Reactivity and Crystallinity in a Zeolite Crystal: Crystallography and Molecular Spectroscopy in One. Angewandte Chemie - International Edition, 2016, 55, 7496-7500.	7.2	14
597	Continuous Flow Pickering Emulsion Catalysis in Droplet Microfluidics Studied with In Situ Raman Microscopy. Chemistry - A European Journal, 2020, 26, 15099-15102.	1.7	14
598	The nanogeochemistry of abiotic carbonaceous matter in serpentinites from the Yap Trench, western Pacific Ocean. Geology, 2021, 49, 330-334.	2.0	14
599	Chemometric analysis of diffuse reflectance spectra of Co2+-exchanged zeolites: spectroscopic fingerprinting of coordination environments. Analytica Chimica Acta, 1997, 348, 267-272.	2.6	13
600	Synthesis of Co-rich CoAPO-CHA molecular sieves in the presence of ethanol and caesium. Chemical Communications, 2000, , 2249-2250.	2.2	13
601	CATALYSIS BY SUPPORTED METAL OXIDES. , 2001, , 613-648.		13
602	Turning a Cr-based heterogeneous ethylene polymerisation catalyst into a selective ethylene trimerisation catalyst. Journal of Molecular Catalysis A, 2007, 269, 5-11.	4.8	13
603	Pd-Catalyzed Telomerization of 1,3-Dienes with Multifunctional Renewable Substrates: Versatile Routes for the Valorization of Biomass-Derived Platform Molecules. Topics in Organometallic Chemistry, 2012, , 45-101.	0.7	13
604	Kβ Detected High-Resolution XANES of Fell and Fell Models of the 2-His-1-Carboxylate Motif: Analysis of the Carboxylate Binding Mode. European Journal of Inorganic Chemistry, 2012, 2012, 1589-1597.	1.0	13
605	Template–Framework Interactions in Tetraethylammoniumâ€Directed Zeolite Synthesis. Angewandte Chemie, 2016, 128, 16278-16282.	1.6	13
606	Synthesis of Hexane-Tetrols and -Triols with Fixed Hydroxyl Group Positions and Stereochemistry from Methyl Glycosides over Supported Metal Catalysts. ACS Sustainable Chemistry and Engineering, 2020, 8, 800-805.	3.2	13
607	Identification of Iron Carbides in Fe(â~Naâ~S)/αâ€Al <sub>2</sub> O <sub>3</sub> Fischerâ€Tropsch Synthesis Catalysts with Xâ€ray Powder Diffractometry and Mössbauer Absorption Spectroscopy. ChemCatChem, 2020, 12, 5121-5139.	1.8	13
608	In Situ Spectroscopy of Calcium Fluoride Anchored Metal–Organic Framework Thin Films during Gas Sorption. Angewandte Chemie - International Edition, 2020, 59, 19545-19552.	7.2	13
609	Inâ€Situ Study on Ni–Mo Stability in a Waterâ€5plitting Device: Effect of Catalyst Substrate and Electric Potential. ChemSusChem, 2020, 13, 3172-3179.	3.6	13
610	Nano-scale insights regarding coke formation in zeolite SSZ-13 subject to the methanol-to-hydrocarbons reaction. Catalysis Science and Technology, 2022, 12, 1220-1228.	2.1	13
611	In Zeolithe eingeschlossene Kupferâ€Histidinâ€Komplexe als Mimetica natürlicher Kupferenzyme. Angewandte Chemie, 1995, 107, 2868-2870.	1.6	12
612	Protonation of the oxygen axial ligand in galactose oxidase model compounds as seen with high resolution X-ray emission experiments and FEFF simulations. Physical Chemistry Chemical Physics, 2011, 13, 5600.	1.3	12

#	Article	IF	CITATIONS
613	Template removal processes within individual micron-sized SAPO-34 crystals: Effect of gas atmosphere and crystal size. Microporous and Mesoporous Materials, 2011, 146, 28-35.	2.2	12
614	Sustainable production of dimethyl adipate by non-heme iron(iii) catalysed oxidative cleavage of catechol. Catalysis Science and Technology, 2015, 5, 2103-2109.	2.1	12
615	NbOx/SiO2 in the gas-phase Beckmann rearrangement of cyclohexanone oxime to ε-caprolactam: Influence of calcination temperature, niobia loading and silylation post-treatment. Applied Catalysis B: Environmental, 2016, 185, 272-280.	10.8	12
616	Highâ€Pressure Operando UVâ€Vis Microâ€6pectroscopy of Coke Formation in Zeoliteâ€based Catalyst Extrudates during the Transalkylation of Aromatics. ChemCatChem, 2020, 12, 5465-5475.	1.8	12
617	Multiâ€Spectroscopic Interrogation of the Spatial Linker Distribution in Defectâ€Engineered Metal–Organic Framework Crystals: The [Cu 3 (btc) 2â^' x (cydc) x ] Showcase. Chemistry - A European Journal, 2020, 26, 3614-3625.	1.7	12
618	Rapid fabrication of MOF-based mixed matrix membranes through digital light processing. Materials Advances, 2021, 2, 2739-2749.	2.6	12
619	New insights into the NH <sub>3</sub> -selective catalytic reduction of NO over Cu-ZSM-5 as revealed by <i>operando</i> spectroscopy. Catalysis Science and Technology, 2022, 12, 2589-2603.	2.1	12
620	In situ Spectroscopy of Catalysts. ChemInform, 2005, 36, no.	0.1	11
621	An Attempt to Selectively Oxidize Methane over Supported Gold Catalysts. Catalysis Letters, 2011, 141, 1429-1434.	1.4	11
622	Pd/TOMPP-catalyzed telomerization of 1,3-butadiene: From biomass-based substrates to new mechanistic insights. Pure and Applied Chemistry, 2012, 84, 1713-1727.	0.9	11
623	A Radical Twist to the Versatile Behavior of Iron in Selective Methane Activation. Angewandte Chemie - International Edition, 2014, 53, 11137-11139.	7.2	11
624	CaO as Dropâ€In Colloidal Catalysts for the Synthesis of Higher Polyglycerols. Chemistry - A European Journal, 2015, 21, 5101-5109.	1.7	11
625	Reactions in Confined Spaces. ChemPhysChem, 2018, 19, 339-340.	1.0	11
626	Integrated Transmission Electron and Singleâ€Molecule Fluorescence Microscopy Correlates Reactivity with Ultrastructure in a Single Catalyst Particle. Angewandte Chemie, 2018, 130, 263-267.	1.6	11
627	Facile Two‧tep Synthesis of Delafossite CuFeO <sub>2</sub> Photocathodes by Ultrasonic Spray Pyrolysis and Hybrid Microwave Annealing. ChemPhotoChem, 2019, 3, 1238-1245.	1.5	11
628	Probing the Effect of Chemical Dopant Phase on Photoluminescence of Monolayer MoS <sub>2</sub> Using in Situ Raman Microspectroscopy. Journal of Physical Chemistry C, 2019, 123, 15738-15743.	1.5	11
629	Nanoweb Surfaceâ€Mounted Metal–Organic Framework Films with Tunable Amounts of Acid Sites as Tailored Catalysts. Chemistry - A European Journal, 2020, 26, 691-698.	1.7	11
630	Reactivity of Single Transition Metal Atoms on a Hydroxylated Amorphous Silica Surface: A Periodic Conceptual DFT Investigation. Chemistry - A European Journal, 2021, 27, 6050-6063.	1.7	11

#	Article	IF	CITATIONS
631	Photoinduced Force Microscopy as an Efficient Method Towards the Detection of Nanoplastics. Chemistry Methods, 2021, 1, 205-209.	1.8	11
632	Dual Fluorescence in Glutathione-Derived Carbon Dots Revisited. Journal of Physical Chemistry C, 2022, 126, 2720-2727.	1.5	11
633	Elucidation of the pre-nucleation phase directing metal-organic framework formation. Cell Reports Physical Science, 2021, 2, 100680.	2.8	11
634	Emerging analytical methods to characterize zeolite-based materials. National Science Review, 2022, 9,	4.6	11
635	Design and applications of a home-built in situ FT-Raman spectroscopic cell. Spectrochimica Acta - Part A: Molecular and Biomolecular Spectroscopy, 2004, 60, 2969-2975.	2.0	10
636	Understanding the Promotion Effect of Lanthanum Oxide on Gold-Based Catalysts in the Partial Oxidation of Methanol by in Situ XAFS and DSC Studies. Journal of Physical Chemistry C, 2011, 115, 15545-15554.	1.5	10
637	Using DFT in Search for Support Effects During Methanol Oxidation on Supported Molybdenum Oxides. ChemPhysChem, 2011, 12, 3281-3290.	1.0	10
638	Photo-spectroscopy of mixtures of catalyst particles reveals their age and type. Faraday Discussions, 2016, 188, 69-79.	1.6	10
639	Electronic and bite angle effects in catalytic C–O bond cleavage of a lignin model compound using ruthenium Xantphos complexes. Catalysis Science and Technology, 2017, 7, 619-626.	2.1	10
640	Highly Oriented Growth of Catalytically Active Zeolite ZSMâ€5 Films with a Broad Range of Si/Al Ratios. Angewandte Chemie, 2017, 129, 11369-11373.	1.6	10
641	Cobaltâ€Ironâ€Manganese Catalysts for the Conversion of Endâ€ofâ€Lifeâ€Tireâ€Derived Syngas into Light Terminal Olefins. Chemistry - A European Journal, 2018, 24, 4597-4606.	1.7	10
642	Stable platinum in a zeolite channel. Nature Materials, 2019, 18, 778-779.	13.3	10
643	Single Particle Assays to Determine Heterogeneities within Fluid Catalytic Cracking Catalysts. Chemistry - A European Journal, 2020, 26, 8546-8554.	1.7	10
644	Disentangling Reaction Processes of Zeolites within Singleâ€Oriented Channels. Angewandte Chemie, 2020, 132, 15632-15636.	1.6	10
645	Visualizing defects and pore connectivity within metal–organic frameworks by X-ray transmission tomography. Chemical Science, 2021, 12, 8458-8467.	3.7	10
646	Zeoliteâ€Tailored Active Site Proximity for the Efficient Production of Pentanoic Biofuels. Angewandte Chemie, 2021, 133, 23906-23914.	1.6	10
647	Understanding Water–Zeolite Interactions: On the Accuracy of Density Functionals. Journal of Physical Chemistry C, 2021, 125, 20261-20274.	1.5	10
648	Monitoring the preparation of (Co)Mo/Al2O3 extrudates using spatially resolved spectroscopic techniques. Studies in Surface Science and Catalysis, 2006, , 175-186.	1.5	9

#	Article	IF	CITATIONS
649	Structure and Basicity of Microporous Titanosilicate ETS-10 and Vanadium-Containing ETS-10. Journal of Physical Chemistry C, 2012, 116, 17124-17133.	1.5	9
650	Mechanistic Study of the Pd/TOMPP-Catalyzed Telomerization of 1,3-Butadiene: Influence of Aromatic Solvents on Bis-Phosphine Complex Formation and Regioselectivity. Organometallics, 2013, 32, 5047-5057.	1.1	9
651	Recalcitrance of Nature: Chemocatalysis for the Production of Biomassâ€Based Building Blocks. ChemSusChem, 2013, 6, 1559-1563.	3.6	9
652	Reaction Mechanism of Pdâ€Catalyzed "COâ€Free―Carbonylation Reaction Uncovered by In Situ Spectroscopy: The Formyl Mechanism. Angewandte Chemie - International Edition, 2021, 60, 3422-3427.	7.2	9
653	Influence of Metalâ€Alkyls on Earlyâ€Stage Ethylene Polymerization over a Cr/SiO <sub>2</sub> Phillips Catalyst: A Bulk Characterization and Xâ€ray Chemical Imaging Study. Chemistry - A European Journal, 2021, 27, 1688-1699.	1.7	9
654	Chemical Imaging of Hierarchical Porosity Formation within a Zeolite Crystal Visualized by Smallâ€Angle Xâ€Ray Scattering and Inâ€5itu Fluorescence Microscopy. Angewandte Chemie - International Edition, 2021, 60, 13803-13806.	7.2	9
655	Monitoring Molecular Weight Changes during Technical Lignin Depolymerization by Operando Attenuated Total Reflectance Infrared Spectroscopy and Chemometrics. ChemSusChem, 2021, 14, 5517-5524.	3.6	9
656	Application of AXAFS Spectroscopy to Transition-Metal Oxides: Influence of the Nearest and Next Nearest Neighbour Shells in Vanadium Oxides. Chemistry - A European Journal, 2007, 13, 5845-5856.	1.7	8
657	Looking inside Catalyst Extrudates with Time-Resolved Surface-Enhanced Raman Spectroscopy (TR-SERS). Applied Spectroscopy, 2012, 66, 1179-1185.	1.2	8
658	"Extracting†the Key Fragment in ETSâ€10 Crystallization and Its Application in AMâ€6 Assembly. Chemistry A European Journal, 2012, 18, 12078-12084.	1.7	8
659	Regioselective Cleavage of Electronâ€Rich Double Bonds in Dienes to Carbonyl Compounds with [Fe(OTf) <sub>2</sub> (mixâ€BPBP)] and a Combination of H <sub>2</sub> O <sub>2</sub> and NalO <sub>4</sub> . European Journal of Inorganic Chemistry, 2015, 2015, 3462-3466.	1.0	8
660	Unraveling the Redox Behavior of a CoMoS Hydrodesulfurization Catalyst: A Scanning Transmission X-ray Microscopy Study in the Tender X-ray Range. Journal of Physical Chemistry C, 2015, 119, 2530-2536.	1.5	8
661	Multi-doped Brookite-Prevalent TiO2 Photocatalyst with Enhanced Activity in the Visible Light. Catalysis Letters, 2018, 148, 2459-2471.	1.4	8
662	Unraveling the Homologation Reaction Sequence of the Zeoliteâ€Catalyzed Ethanolâ€ŧoâ€Hydrocarbons Process. Angewandte Chemie, 2019, 131, 3948-3952.	1.6	8
663	Controlling the Depolymerization of Paraformaldehyde with Pd–Phosphine Complexes. Chemistry - A European Journal, 2020, 26, 5297-5302.	1.7	8
664	Deactivation of Cuâ€Exchanged Automotiveâ€Emission NH 3 â€SCR Catalysts Elucidated with Nanoscale Resolution Using Scanning Transmission Xâ€ray Microscopy. Angewandte Chemie, 2020, 132, 15740-15747.	1.6	8
665	Identification of Photoexcited Electron Relaxation in a Cobalt Phosphide Modified Carbon Nitride Photocatalyst. ChemPhotoChem, 2021, 5, 330-334.	1.5	8
666	Plastic Waste Conversion over a Refinery Waste Catalyst. Angewandte Chemie, 2021, 133, 16237-16244.	1.6	8

#	Article	IF	CITATIONS
667	Mechanistic Insights into the Lanthanide-Catalyzed Oxychlorination of Methane as Revealed by Operando Spectroscopy. ACS Catalysis, 2021, 11, 10574-10588.	5.5	8
668	Bis(μ-OXO)dicopper as intermediate in the catalytic decomposition of No over Cu-ZSM-5. Studies in Surface Science and Catalysis, 2004, 154, 2449-2457.	1.5	7
669	Diagnosing the Internal Architecture of Zeolite Ferrierite. ChemPhysChem, 2018, 19, 367-372.	1.0	7
670	Capturing the Genesis of an Active Fischer–Tropsch Synthesis Catalyst with Operando Xâ€ray Nanospectroscopy. Angewandte Chemie, 2018, 130, 12133-12138.	1.6	7
671	Uniformly Oriented Zeolite ZSMâ€5 Membranes with Tunable Wettability on a Porous Ceramic. Angewandte Chemie, 2018, 130, 12638-12642.	1.6	7
672	Hexane-1,2,5,6-tetrol as a Versatile and Biobased Building Block for the Synthesis of Sustainable (Chiral) Crystalline Mesoporous Polyboronates. ACS Sustainable Chemistry and Engineering, 2019, 7, 13430-13436.	3.2	7
673	Upscaling Effects on Alkali Metalâ€Grafted Ultrastable Y Zeolite Extrudates for Modeled Catalytic Deoxygenation of Bioâ€oils. ChemCatChem, 2021, 13, 1951-1965.	1.8	7
674	Wasteâ€Derived Copperâ€Lead Electrocatalysts for CO <sub>2</sub> Reduction. ChemCatChem, 2022, 14, .	1.8	7
675	Chemometric analysis of diffuse reflectance spectra of CoA zeolites: Spectroscopic fingerprinting of Co2+-sites. Studies in Surface Science and Catalysis, 1997, , 623-630.	1.5	6
676	Synthesis of Co-Rich CoAPO-5 Molecular Sieves: A Comparison between Glycerol and Water as Solvent. Journal of Nanoscience and Nanotechnology, 2003, 3, 271-275.	0.9	6
677	The effect of chemical composition and structure on XPS binding energies in zeolites. Studies in Surface Science and Catalysis, 2004, , 1385-1392.	1.5	6
678	New Highly Mixed Phases in Ball-Milled Cu/ZnO Catalysts as Established by EXAFS and XANES. AIP Conference Proceedings, 2007, , .	0.3	6
679	The Epoxidation of Propene over Gold Nanoparticle Catalysts. , 2008, , 339-354.		6
680	Conceptual chemistry approach towards the support effect in supported vanadium oxides: Valence bond calculations on the ionicity of vanadium catalysts. Catalysis Today, 2011, 177, 3-11.	2.2	6
681	Techniques Coupling for Catalyst Characterisation. , 2012, , 1075-1117.		6
682	Breakthroughs in Hard Xâ€ray Diffraction: Towards a Multiscale Science Approach in Heterogeneous Catalysis. Angewandte Chemie - International Edition, 2014, 53, 8556-8558.	7.2	6
683	Xâ€ray Excited Optical Fluorescence and Diffraction Imaging of Reactivity and Crystallinity in a Zeolite Crystal: Crystallography and Molecular Spectroscopy in One. Angewandte Chemie, 2016, 128, 7622-7626.	1.6	6

684 Operando EXAFS and XANES of Catalytic Solids and Related Materials. , 2017, , 167-191.

6

#	Article	IF	CITATIONS
685	Efficient and Highly Transparent Ultraâ€Thin Nickelâ€Iron Oxyâ€hydroxide Catalyst for Oxygen Evolution Prepared by Successive Ionic Layer Adsorption and Reaction. ChemPhotoChem, 2019, 3, 1050-1054.	1.5	6
686	Formation and Functioning of Bimetallic Nanocatalysts: The Power of Xâ€ray Probes. Angewandte Chemie, 2019, 131, 13354-13364.	1.6	6
687	In Situ Spectroscopy of Calcium Fluoride Anchored Metal–Organic Framework Thin Films during Gas Sorption. Angewandte Chemie, 2020, 132, 19713-19720.	1.6	6
688	Femtosecond Charge Density Modulations in Photoexcited CuWO <sub>4</sub> . Journal of Physical Chemistry C, 2021, 125, 7329-7336.	1.5	6
689	Operando Shellâ€Isolated Nanoparticleâ€Enhanced Raman Spectroscopy of the NO Reduction Reaction over Rhodiumâ€Based Catalysts. ChemPhysChem, 2021, 22, 1595-1602.	1.0	6
690	X-ray nanotomography uncovers morphological heterogeneity in a polymerization catalyst at multiple reaction stages. Chem Catalysis, 2021, 1, 1413-1426.	2.9	6
691	Understanding the Effects of Binders in Gas Sorption and Acidity of Aluminium Fumarate Extrudates. Chemistry - A European Journal, 2022, 28, .	1.7	6
692	An integrated approach to the key parameters in methanol-to-olefins reaction catalyzed by MFI/MEL zeolite materials. Chinese Journal of Catalysis, 2022, 43, 1879-1893.	6.9	6
693	Classification-based motion analysis of single-molecule trajectories using DiffusionLab. Scientific Reports, 2022, 12, .	1.6	6
694	On the intergrowth structure of zeolite crystals as revealed by wide field and confocal fluorescence microscopy of the template removal processes. Studies in Surface Science and Catalysis, 2008, 174, 757-762.	1.5	5
695	In-situ Scanning Transmission X-ray Microscopy of catalytic materials under reaction conditions. Journal of Physics: Conference Series, 2009, 190, 012161.	0.3	5
696	Synthesis and Morphology Control of AMâ€6 Nanofibers with Tailored â€Vâ€Oâ€V―Intermediates. Chemistry - A European Journal, 2013, 19, 14200-14204.	1.7	5
697	Zeolites shine bright. Nature Materials, 2016, 15, 933-934.	13.3	5
698	Nanoscale Chemical Imaging of Coking Mechanisms in a Zeolite ZSM-5 Crystal by Atom Probe Tomography. Microscopy and Microanalysis, 2017, 23, 674-675.	0.2	5
699	Behavior of a Metal Organic Framework Thinâ€Film at Elevated Temperature and Pressure as Studied with an Autoclaveâ€Inserted Atomic Force Microscope. ChemPhysChem, 2018, 19, 2397-2404.	1.0	5
700	Synthesis and Characterization of Ru‣oaded Anodized Aluminum Oxide for Hydrogenation Catalysis. ChemistryOpen, 2019, 8, 532-538.	0.9	5
701	Nickel Poisoning of a Cracking Catalyst Unravelled by Singleâ€Particle Xâ€ray Fluorescenceâ€Diffractionâ€Absorption Tomography. Angewandte Chemie, 2020, 132, 3950-3955.	1.6	5
702	Basicity and Electrolyte Composition Dependent Stability of Niâ€Feâ€S and Niâ€Mo Electrodes during Water Splitting. ChemPhysChem, 2020, 21, 518-524.	1.0	5

#	Article	IF	CITATIONS
703	Single catalyst particle diagnostics in a microreactor for performing multiphase hydrogenation reactions. Faraday Discussions, 2021, 229, 267-280.	1.6	5
704	In situ Nanoscale Infrared Spectroscopy of Water Adsorption on Nanoislands of Surfaceâ€Anchored Metalâ€Organic Frameworks. Angewandte Chemie, 2021, 133, 1644-1648.	1.6	5
705	5-Hydroxy-2-Methylfurfural from Sugar Beet Thick Juice: Kinetic and Modeling Studies. ACS Sustainable Chemistry and Engineering, 2021, 9, 2626-2638.	3.2	5
706	Influence of Pore Structure and Metalâ€Node Geometry on the Polymerization of Ethylene over Crâ€Based Metal–Organic Frameworks. Chemistry - A European Journal, 2021, 27, 5769-5781.	1.7	5
707	Coordination Chemistry in Zeolites. Topics in Inclusion Science, 1995, , 185-213.	0.5	5
708	Mimicking industrial aging in fluid catalytic cracking: A correlative microscopy approach to unravel inter-particle heterogeneities. Journal of Catalysis, 2021, 404, 634-646.	3.1	5
709	Unravelling Channel Structure–Diffusivity Relationships in Zeolite ZSMâ€5 at the Singleâ€Molecule Level. Angewandte Chemie, 2022, 134, .	1.6	5
710	Favoring the Methane Oxychlorination Reaction over EuOCl by Synergistic Effects with Lanthanum. ACS Catalysis, 2022, 12, 5698-5710.	5.5	5
711	Hole Dynamics in Photoexcited Hematite Studied with Femtosecond Oxygen K-edge X-ray Absorption Spectroscopy. Journal of Physical Chemistry Letters, 2022, 13, 4207-4214.	2.1	5
712	Unraveling the Structure of Mn-Promoted Co/TiO2 Fischer-Tropsch Catalysts by In Situ X-Ray Absorption Spectroscopy. AIP Conference Proceedings, 2007, , .	0.3	4
713	Observing the Influence of X-Rays on Aqueous Copper Solutions by In Situ Combined Video/XAFS/UV-Vis Spectroscopy. AIP Conference Proceedings, 2007, , .	0.3	4
714	Multi-Technique In Situ Approach Towards the Study of Catalytic Solids at Work Using Synchrotron Radiation. Synchrotron Radiation News, 2009, 22, 22-30.	0.2	4
715	Cu-Zeolite Selective Catalytic Reduction Catalysts for NOx Conversion. , 2016, , 433-450.		4
716	Designing new catalysts: synthesis of new active structures: general discussion. Faraday Discussions, 2016, 188, 131-159.	1.6	4
717	Mechanistic Insights into the Conversion of Biorenewable Levoglucosanol to Dideoxysugars. ACS Sustainable Chemistry and Engineering, 2020, 8, 16339-16349.	3.2	4
718	Tuning the Redox Chemistry of a Cr/SiO <sub>2</sub> Phillips Catalyst for Controlling Activity, Induction Period and Polymer Properties. ChemPhysChem, 2020, 21, 1665-1674.	1.0	4
719	Nature of cobalt species during the <i>in situ</i> sulfurization of Co(Ni)Mo/Al <sub>2</sub> O <sub>3</sub> hydrodesulfurization catalysts. Journal of Synchrotron Radiation, 2019, 26, 811-818.	1.0	4
720	Promotion effects in the oxidation of CO over zeolite-supported Pt nanoparticles. Studies in Surface Science and Catalysis, 2005, , 1239-1246.	1.5	3

#	Article	IF	CITATIONS
721	Mn and Fe ions and oxo clusters in ZSM-5: pushing the limits of X-ray spectroscopy. Studies in Surface Science and Catalysis, 2007, , 796-799.	1.5	3
722	ED-XAS Data Reveal In-situ Time-Resolved Adsorbate Coverage on Supported Molybdenum Oxide Catalysts during Propane Dehydrogenation. AIP Conference Proceedings, 2007, , .	0.3	3
723	An eye on the inside of zeolite crystals in the act: Studying BrĂุnsted acidity with in-situ micro-spectroscopy. Studies in Surface Science and Catalysis, 2008, , 21-32.	1.5	3
724	On the Microdistributions of Crâ€lon Complexes within mmâ€Sized γâ€Al <sub>2</sub> O <sub>3</sub> Catalyst Bodies upon Impregnation as Studied by UV/Vis and Raman Microspectroscopy. ChemCatChem, 2012, 4, 217-227.	1.8	3
725	Separation of Time-Resolved Phenomena in Surface-Enhanced Raman Scattering of the Photocatalytic Reduction ofp-Nitrothiophenol. ChemPhysChem, 2015, 16, 489-489.	1.0	3
726	Bridging model and real catalysts: general discussion. Faraday Discussions, 2016, 188, 565-589.	1.6	3
727	Cathodic Electrodeposition of Niâ^'Mo on Semiconducting NiFe <sub>2</sub> O <sub>4</sub> for Photoelectrochemical Hydrogen Evolution in Alkaline Media. ChemSusChem, 2018, 11, 1374-1381.	3.6	3
728	Magnetophoretic Sorting of Single Catalyst Particles. Angewandte Chemie, 2018, 130, 10749-10754.	1.6	3
729	Extending Surfaceâ€Enhanced Raman Spectroscopy to Liquids Using Shellâ€Isolated Plasmonic Superstructures. Chemistry - A European Journal, 2019, 25, 15772-15778.	1.7	3
730	Elucidating Zeolite Channel Geometry–Reaction Intermediate Relationships for the Methanolâ€ŧoâ€Hydrocarbon Process. Angewandte Chemie, 2020, 132, 20199-20205.	1.6	3
731	Disk-Shaped Cobalt Nanocrystals as Fischer–Tropsch Synthesis Catalysts Under Industrially Relevant Conditions. Topics in Catalysis, 2020, 63, 1398-1411.	1.3	3
732	Single Particle Assays to Determine Heterogeneities within Fluid Catalytic Cracking Catalysts. Chemistry - A European Journal, 2020, 26, 8482-8482.	1.7	3
733	Reaction Mechanism of Pdâ€Catalyzed "COâ€Free―Carbonylation Reaction Uncovered by In Situ Spectroscopy: The Formyl Mechanism. Angewandte Chemie, 2021, 133, 3464-3469.	1.6	3
734	Crowded catalyst, better catalyst. National Science Review, 2021, 8, nwab141.	4.6	3
735	Deactivation and regeneration of solid acid and base catalyst bodies used in cascade for bio-oil synthesis and upgrading. Journal of Catalysis, 2022, 405, 641-651.	3.1	3
736	Production of Hexane-1,2,5,6-tetrol from Biorenewable Levoglucosanol over Pt-WO <sub><i>x</i></sub> /TiO <sub>2</sub> . ACS Sustainable Chemistry and Engineering, 2021, 9, 16123-16132.	3.2	3
737	Synthesis and characterization of zeolite encaged enzyme-mimetic copper histidine complexes. Studies in Surface Science and Catalysis, 2000, , 287-293.	1.5	2
738	In situ X-Ray Absorption of Co/Mn/TiO2 Catalysts for Fischer—Tropsch Synthesis ChemInform, 2004, 35, no.	0.1	2

#	Article	IF	CITATIONS
739	Understanding the crystallisation processes leading to the formation of microporous aluminophosphates. Studies in Surface Science and Catalysis, 2007, 170, 748-755.	1.5	2
740	Bio-inspired manipulation of catalytic sites via immobilization of metal ion complexes in zeolites. Studies in Surface Science and Catalysis, 2007, 170, 1546-1551.	1.5	2
741	Catalyst design from theory to practice: general discussion. Faraday Discussions, 2016, 188, 279-307.	1.6	2
742	Solid catalysts under the spotlight. Nature Catalysis, 2018, 1, 101-102.	16.1	2
743	Micro-Spectroscopy to Interrogate Solid Catalysts at Work. , 2018, , 304-320.		2
744	Communicating catalysts. Nature Chemistry, 2018, 10, 580-582.	6.6	2
745	Kinetics of Lifetime Changes in Bimetallic Nanocatalysts Revealed by Quick Xâ€ray Absorption Spectroscopy. Angewandte Chemie, 2018, 130, 12610-12614.	1.6	2
746	Preface: Catalysis for Valorization of Biomass and Biomass-derived Platform Molecules (18th NCC). Catalysis Today, 2019, 319, 1.	2.2	2
747	Transforming inactive coke molecules into active intermediates in zeolites. Joule, 2021, 5, 757-759.	11.7	2
748	Chemical Imaging of Hierarchical Porosity Formation within a Zeolite Crystal Visualized by Smallâ€Angle Xâ€Ray Scattering and In‣itu Fluorescence Microscopy. Angewandte Chemie, 2021, 133, 13922-13925.	1.6	2
749	Separation and Purification of Hydrocarbons with Porous Materials. Angewandte Chemie, 2021, 133, 19078-19097.	1.6	2
750	Fresh evidence challenges the consensus view of active sites in an industrial catalyst. Nature, 2020, 586, 678-679.	13.7	2
751	Using Biomass Gasification Mineral Residue as Catalyst to Produce Light Olefins from CO, CO <sub>2</sub> , and H <sub>2</sub> Mixtures. ChemSusChem, 2022, 15, e202200436.	3.6	2
752	Using Biomass Gasification Mineral Residue as Catalyst to Produce Light Olefins from CO, CO <sub>2</sub> , and H <sub>2</sub> Mixtures. ChemSusChem, 2022, 15, e202200851.	3.6	2
753	Crossing the Interfaces of Catalysis. ChemCatChem, 2009, 1, 7-7.	1.8	1
754	Triazacyclophane (TAC)-scaffolded histidine and aspartic acid residues as mimics of non-heme metalloenzyme active sites. Organic and Biomolecular Chemistry, 2012, 10, 1088-1092.	1.5	1
755	New Editorial Board Members: Refreshing our Catalyst!. ChemCatChem, 2013, 5, 6-8.	1.8	1
756	Data-processing strategies for nano-tomography with elemental specification. Proceedings of SPIE, 2013, , .	0.8	1

#	Article	IF	CITATIONS
757	Correction to Role of Magnesium Silicates in Wet-Kneaded Silica-Magnesia Catalysts for the Lebedev Ethanol-to-Butadiene Process. ACS Catalysis, 2016, 6, 7685-7685.	5.5	1
758	Design and characterization of a microreactor for monodisperse catalytic droplet generation at both elevated temperatures and pressures. , 2017, , .		1
759	Frontispiece: Thermally Stable TiO <sub>2</sub> ―and SiO <sub>2</sub> â€Shellâ€Isolated Au Nanoparticles for In Situ Plasmonâ€Enhanced Raman Spectroscopy of Hydrogenation Catalysts. Chemistry - A European Journal, 2018, 24, .	1.7	1
760	Nanoskalige chemische Bildgebung von Zeolithen durch Atomsondentomographie. Angewandte Chemie, 2018, 130, 10580-10593.	1.6	1
761	Advances in X-ray Micro-Spectroscopy of Heterogeneous Catalysts. Microscopy and Microanalysis, 2018, 24, 412-415.	0.2	1
762	Extending Surfaceâ€Enhanced Raman Spectroscopy to Liquids Using Shellâ€Isolated Plasmonic Superstructures. Chemistry - A European Journal, 2019, 25, 15706-15706.	1.7	1
763	Two-in-One Catalyst Turns Carbon Dioxide in Base Chemicals. CheM, 2020, 6, 3167-3169.	5.8	1
764	Advanced approaches: general discussion. Faraday Discussions, 2021, 229, 378-421.	1.6	1
765	Crystal Phase Effects on the Gasâ€Phase Ketonization of Small Carboxylic Acids over TiO 2 Catalysts. ChemSusChem, 2021, 14, 2634-2634.	3.6	1
766	Monitoring Aqueous Phase Reactions by Operando ATRâ€ <b>I</b> R Spectroscopy at High Temperature and Pressure: A Biomass Conversion Showcase. Chemistry Methods, 0, , .	1.8	1
767	New insights into the biphasic "CO-free―Pauson–Khand cyclisation reaction through combined <i>in situ</i> spectroscopy and multiple linear regression modelling. Catalysis Science and Technology, 2021, 11, 1626-1636.	2.1	1
768	Space and Time-Resolved Spectroscopy of Catalyst Bodies. , 0, , 201-216.		1
769	Tip-enhanced Raman spectroscopy applications: from graphene to heterogeneous catalysis. , 2018, , .		1
770	Chemistry, Spectroscopy and the Role of Supported Vanadium Oxides in Heterogeneous Catalysis. ChemInform, 2003, 34, no.	0.1	0
771	Surface Acidity and Basicity of La2O3, LaOCl, and LaCl3 Characterized by IR Spectroscopy, TPD, and DFT Calculations ChemInform, 2004, 35, no.	0.1	Ο
772	Promotion Effects in the Oxidation of CO over Zeolite-Supported Pt Nanoparticles ChemInform, 2005, 36, no.	0.1	0
773	Quantitative CARS Of Chemistry In Confinement. , 2010, , .		0
774	Editorial: Solving the Material and Energy Challenges of the Future. ChemCatChem, 2011, 3, 619-621.	1.8	0

#	Article	IF	CITATIONS
775	An eye on the inside: imaging of catalytic particles under reaction conditions. Acta Crystallographica Section A: Foundations and Advances, 2012, 68, s44-s44.	0.3	0
776	The Seventeenth International Symposium on Relations Between Homogeneous and Heterogeneous Catalysis Utrecht July 12–15 2015. Topics in Catalysis, 2016, 59, 1669-1670.	1.3	0
777	Photoelectrochemistry: Enhanced Photoresponse of FeS2 Films: The Role of Marcasite-Pyrite Phase Junctions (Adv. Mater. 43/2016). Advanced Materials, 2016, 28, 9656-9656.	11.1	0
778	Application of novel catalysts: general discussion. Faraday Discussions, 2016, 188, 399-426.	1.6	0
779	Innenrücktitelbild: Highly Oriented Growth of Catalytically Active Zeolite ZSMâ€5 Films with a Broad Range of Si/Al Ratios (Angew. Chem. 37/2017). Angewandte Chemie, 2017, 129, 11427-11427.	1.6	0
780	Rücktitelbild: Integrated Transmission Electron and Singleâ€Molecule Fluorescence Microscopy Correlates Reactivity with Ultrastructure in a Single Catalyst Particle (Angew. Chem. 1/2018). Angewandte Chemie, 2018, 130, 366-366.	1.6	0
781	Frontispiece: Matrix Effects in a Fluid Catalytic Cracking Catalyst Particle: Influence on Structure, Acidity, and Accessibility. Chemistry - A European Journal, 2020, 26, .	1.7	0
782	Titelbild: Elucidating Zeolite Channel Geometry–Reaction Intermediate Relationships for the Methanolâ€ŧoâ€Hydrocarbon Process (Angew. Chem. 45/2020). Angewandte Chemie, 2020, 132, 19893-19893.	1.6	0
783	THEORETICAL MODELLING OF FUNCTIONAL MATERIALS. , 2021, , .		0
784	TOWARDS IN-SILICO DESIGN OF FUNCTIONAL MATERIALS. , 2021, , .		0
785	Innentitelbild: Chemical Imaging of Hierarchical Porosity Formation within a Zeolite Crystal Visualized by Smallâ€Angle Xâ€Ray Scattering and Inâ€Situ Fluorescence Microscopy (Angew. Chem. 25/2021). Angewandte Chemie, 2021, 133, 13802-13802.	1.6	0
786	Photoinduced Force Microscopy as an Efficient Method Towards the Detection of Nanoplastics. Chemistry Methods, 2021, 1, 204-204.	1.8	0
787	Nanoscale Chemical Imaging in Zeolite Catalysts by Atom Probe Tomography. Microscopy and Microanalysis, 2021, 27, 984-985.	0.2	0
788	Chapter 7. Catalytic Conversion of Lignin-derived Aromatic Compounds into Chemicals. RSC Energy and Environment Series, 2018, , 159-198.	0.2	0
789	OPERANDO SPECTROSCOPY OF A CATALYTIC SOLID: TOWARDS A MOLECULAR MOVIE. , 2018, , .		0
790	Probing the Dynamics of CO2 Electroreduction with Time-Resolved Raman Spectroscopy. , 0, , .		0
791	Near unity electrochemical CO2 to CO conversion over Sn-doped CuO nanoparticles with prolonged stability. , 0, , .		0
792	Rücktitelbild: Unravelling Channel Structure–Diffusivity Relationships in Zeolite ZSMâ€5 at the Singleâ€Molecule Level (Angew. Chem. 5/2022). Angewandte Chemie, 2022, 134, .	1.6	0